Annu. Rev. Nucl. Part. Sci. 1995. 45:543–90

LOW-RADIOACTIVITY BACKGROUND TECHNIQUES

G. Heusser

Max-Planck-Institut für Kernphysik, P.O. Box 103 980, D-69029 Heidelberg, Germany

---

CONTENTS

KEY WORDS: low-level, rare events, solar neutrinos, $\beta\beta$ decay, dark matter

ABSTRACT

Interest is increasing in nonaccelerator physics with very low event rates, e.g. in experiments on solar neutrinos, double beta ($\beta\beta$) decay, and dark matter search. The basic sources of background in the detection of ionizing radiation are discussed, with particular emphasis on the cosmic ray–induced component. Their

0163-8998/95/1201-0543$5.00

reduction through shielding, material selection, underground operation, and various discrimination methods is elaborated and occasionally illustrated for the case of Ge spectrometry. The state-of-the-art techniques as they are applied in some advanced rare-event experiments are then reviewed.

1. INTRODUCTION

Subsequent to past discoveries in physics due to strong effects and thus a "large signal," many open questions in modern physics can only be further addressed with techniques able to filter a weak signal out of background and noise. This is especially true for experiments based on the detection of ionizing particles. In this case, spurious counts resulting from environmental radioactivity; from intrinsic contamination of the target, detector, and shielding material; from airborne activity (radon); from cosmic rays; or from neutrons can obscure the signal counts of interest.

Ionization detection has its origins in the ionization chambers of the nineteenth century. It rapidly progressed with the invention of Geiger-Müller (1928) and proportional ($\sim$1940) counters. In 1948, NaI(Tl) scintillation crystals came into use and provided better conditions for γ-ray detection. Since then, scintillation counting has been extended to many other inorganic crystals [e.g. CsI(Tl), ($Bi_4Ge_3O_{12}$)(BGO), $CdWO_4$,...] and organic-based liquids and plastics. Liquid scintillations counting has found wide application, mainly in the life sciences.

In the beginning of the 1960s, Ge(Li) and Si(Li) crystals—and later intrinsic [or high purity] Ge crystals—revolutionized the nuclear sector because of their high energy resolution. Cryogenic detectors, the latest generation in detector technology under development in different laboratories around the world, reach even a higher energy resolution, since they are able to register phonons, the thermal debris of the ionizing event. However, their application might be rather limited because of their long integration times.

In many fields, the above-mentioned detectors are applied to investigations with very low event rates. Therefore, these detectors require a low background. The problems to be addressed are vast and steadily increasing, especially in life and environmental sciences, in geophysics, in nuclear and subnuclear physics, and most recently, in particle astrophysics.

1.1 *Rare Event Experiments*

The most advances have been made in experiments searching for solar neutrinos, double beta ($\beta\beta$) decay, and dark matter particles. Here, event rates as low as a few per day or even a few per year are anticipated. One common scientific motivation in this class of experiments is the determination of neutrino properties, in

particular whether the neutrino has a nonvanishing rest mass. Although written in popular style, a comprehensive and detailed historical overview of neutrino physics can be found in Reference 1.

1.1.1 SOLAR NEUTRINOS The primary aim of solar neutrino experiments is to verify the chain of fusion reactions fueling the Sun that is predicted by the standard solar model (SSM) calculations (2, 3). Only the neutrinos emitted in these reactions can transmit this information directly from the core of the Sun to us. The extremely weak interaction with the overlying solar matter reduces the neutrino flux by only about 3%. Detection is either by neutrino capture reactions such as $^{37}Cl(\nu_e, e^-)^{37}Ar$ or $^{71}Ga(\nu_e, e^-)^{71}Ge$ in radiochemical experiments or by neutrino-electron elastic scattering in a direct counting experiment (4). In the former, the product isotope is extracted from the target solution (C_2Cl_4 or $GaCl_3$ solution) after some accumulation time and counted in miniature proportional counters. In the latter, the scattered electrons are measured by their Čerenkov light with a large photomultiplier array in a big water tank. In both types of experiments, large masses of target materials are required in order to obtain signal rates of about one event per day. These materials need to be radiopure and must be placed deep underground so as to keep side reactions or multiplier trigger rates below the neutrino signal. Radiochemical experiments present the additional challenge of counting the few radioactive atoms at extremely low-level conditions.

Ongoing and future solar neutrino experiments were reviewed recently in this series and elsewhere (5). The solar neutrino problem of a strong deficit in high-energy ^8B neutrinos and a moderate one in low-energy neutrinos has not changed notably since then, except that the latter deficit has become more significant as a result of accumulated higher statistics in the Ga experiments [GALLEX (6) and SAGE (7)]. This deficit against SSM calculations was recently interpreted (8) in terms of a severe depression of ^7Be neutrinos. GALLEX has performed the first successful test of a solar neutrino detector with a man-made radioactive source of electron neutrinos (9).

1.1.2 DOUBLE BETA ($\beta\beta$) DECAY Another way to search for a finite neutrino rest mass is through the observation of neutrinoless $\beta\beta$ decay. $\beta\beta$ decay (for a recent review see Reference 11) can occur in three modes: two-neutrino decay (2ν), neutrinoless decay (0ν), and decay with the emission of a Majoron. Of these, the neutrinoless mode is the most interesting. The observation of this decay would imply lepton number violation, a finite (Majorana) mass, and/or a right-handed admixture to the generally left-handed weak interaction. In direct counting experiments, the "source equal to the detector" approach is the most powerful. It allows the use of large source masses to probe this extremely rare

process with expected half-lives of more than 10^{21} years. Pioneered by Fiorini (12), Ge diodes are ideally suited for this task, especially since Ge enriched in ^{76}Ge ($\beta\beta$-active isotope) came into use (13, 14). The high energy resolution of Ge detectors facilitates the detection of a monoenergetic line—the distinctive signature of the 0ν electron energy spectrum.

Approximately 40 $\beta\beta$ experiments are in preparation or in progress (11). The background reduction methods of a few representative programs are outlined in Section 5.2. So far, no evidence for the 0ν decay channel has been reported, but upper mass limits for the effective (Majorana) mass below 1 eV (14) have been noted. To date, two-neutrino decay has been observed in nine nuclei. This process provides a useful test of the theoretical models involved in the calculation of nuclear matrix elements.

1.1.3 DARK MATTER The substantial observational evidence that more than 90% of the mass in the universe may be invisible has prompted an intense search for dark matter candidates (15, 16). The galactic dark matter may eventually be composed of neutral weakly interacting massive particles (WIMPs). These particles would be identifiable by their elastic scattering on nuclei.

Here, low-background detectors with an energy threshold as low as possible are needed. In addition to conventional detectors such as Ge, Si, and NaI(Tl), cryogenic calorimeters will also be used. These latter detectors are fully sensitive to low-energy nuclear recoil, whereas ionization and scintillation detectors register only a fraction of the deposited energy. Through the use of conventional detectors, certain candidates of nonbaryonic dark matter, notably heavy Dirac neutrinos within a large mass range, have already been ruled out.

2. SOURCES OF BACKGROUND RADIATION

In counting experiments, the sensitivity is, approximately, directly proportional to the signal rate but inversely proportional only to the square root of the background rate. Because signal rates in the experiments mentioned above are mostly limited by experimental parameters or for economic reasons, the less effective route of background reduction must be followed. The sources of background must be thoroughly understood before measures can be taken. Although they vary from experiment to experiment, the background sources can be roughly divided into the following components, listed in approximate order of importance: (*a*) environmental radioactivity, (*b*) radioimpurities in detector and shield material, (*c*) Rn and its progenies, (*d*) cosmic rays, and (*e*) neutrons from natural fission and (α, n) reactions. The optimization by reduction of these sources is meaningful only in context. The degree of radiopurity in the detector assembly is crucial for the level of improvement that can be achieved

for the other components. Interrelations also exist. For instance, the choice and thickness of material for the shield against external γ radiation influence the cosmic ray–induced background. Throughout this article, Ge spectrometry is occasionally used to illustrate the impact of the individual components and the required counter measures (17, 18).

2.1 *Environmental Radioactivity*

Radionuclides in our environment are of three general types: primordial, cosmogenic, and anthropogenic (man-made).

The γ radiation against which we must shield our detectors is comprised almost exclusively of photons from the U and Th decay series and from ^{40}K decay. At sea level it corresponds typically to 10 photons $cm^{-2}s^{-1}$ (> 50 keV) at 1 m above ground (19). The cosmic ray photon flux density is only a small fraction ($\leq 1\%$) of it (20). All other primordial radionuclides, including the actinium series are negligible in this respect. Average concentrations in the continental upper crust are: ^{40}K, 850 $Bq \cdot kg^{-1}$; ^{87}Rb (no γ), 100 $Bq \cdot kg^{-1}$; ^{232}Th, 44 $Bq \cdot kg^{-1}$; and ^{238}U, 36 $Bq \cdot kg^{-1}$ (20). In soil, these concentrations are about half as large except for that of Th, which remains the same. Variations in concentration are substantial, with the highest activities found in granites and pegmatites.

For the purpose of comparison, the concentration of radionuclides is generally given in this article in $Bq \cdot kg^{-1}$ or subunits thereof. This also applies to primordial nuclides for which the measurement of concentrations by weight is more common. Conversion factors are as follows:

$1\ Bq\,^{238}U\,kg^{-1} \triangleq 81 \cdot 10^{-9} g\,U\,g^{-1}$ (81 ppb U),

$1\ Bq\,^{232}Th\,kg^{-1} \triangleq 246 \cdot 10^{-9} g\,Th\,g^{-1}$ (246 ppb Th),

$1\ Bq\,^{40}K\,kg^{-1} \triangleq 32.3 \cdot 10^{-6} g\,K\,g^{-1}$ (32.3 ppm K),

$1\ pCi = 37\ mBq$.

Secular equilibrium in the decay series (where activities of all daughter nuclides are equal to the activity of their respective parents) is rarely achieved in most surface and near-surface geological environments, since nuclides of the chain are subject to migration as a result of physical or chemical processes (21). In particular, Rn (Section 2.3), an intermediate member of all three decay series, may escape from the solid matrix either by recoil on ejection of the α particle or by diffusion. In this way, about 1300 Bq ^{222}Rn $m^{-2}day^{-1}$ (21) are released from the Earth's land surface into the atmosphere. The longer-living progeny of Rn, ^{210}Pb, is readily attached to aerosols and finally deposited on the surface by washout and dry deposition.

In laboratory buildings, the concentrations of primordials are comparable unless the building material has been especially selected or wood has been

used. Often a major problem is finding low-activity cement for the concrete constructions. Sulfurcrete made with sulfur and a polymer as binder contains only about 45 mBq ^{232}Th kg^{-1} and 110 mBq ^{238}U kg^{-1} (22).

Higher concentrations of U and Th require a thicker shield against γ radiation. In addition they cause higher levels of Rn and neutrons [from spontaneous fission and from (α, n) reactions]. Typical spectra as measured with unshielded Ge detectors are shown in Figures 6 and 8 (Sections 4.1 and 5.2, respectively). These spectra feature all the γ lines of the U and Th series and of K.

The most significant cosmic ray–produced radionuclides in the atmosphere and hence in our environment are ^{14}C, ^{3}H, ^{7}Be, ^{10}Be, and ^{36}Cl. [For a more complete list see Lal & Peters (23).] Contributions from the lithosphere and hydrosphere are negligible (24) because of the exponential decrease of cosmic ray secondaries. The total activity inventory of cosmogenic radionuclides in the upper soil layer, including the precipitated atmospheric products, is only in the permil range of the primordial activity. Therefore, these radionuclides need attention only in detectors based on substances containing C, H, Be, or Cl, such as scintillation or gas counters. The latter can also be affected by cosmic ray–derived rare gases such as ^{37}Ar, ^{39}Ar, ^{42}Ar, ^{85}Kr (see also below), and ^{81}Kr. A special contamination problem for Si detectors can result from ^{32}Si (25). In situ cosmic ray activation is addressed in Section 3.1.

Nuclear weapons testing has added major quantities to the natural inventories of ^{3}H and ^{14}C. It has also added other so-called anthropogenic radionuclides such as ^{137}Cs and ^{90}Sr to our global environment. The Chernobyl accident raised the concentration of ^{137}Cs appreciably in some places. Almost all surfaces exposed to the plume in 1986 became contaminated. It is therefore essential to check materials from that time before using them in low-background experiments.

The release of ^{85}Kr from nuclear fuel reprocessing plants results in a constant yearly increase of this gas in the atmosphere, with a long-term average rate of about 30 mBq $\cdot$ m^{-3} air (26). Its present concentration in the western hemisphere is 1.1 Bq $\cdot$ m^{-3} air (26). Other rare gases that are processed from air also contain this concentration in their krypton fraction. The Xe radioisotopes ^{131m}Xe, ^{133}Xe, and ^{135}Xe are short-lived and consequently not enriched in the atmosphere.

2.2 *Radioimpurities in Detector and Shield Material*

The omnipresence of primordial radionuclides in ores and other raw materials results in a wide range of contamination in the final product. With some exceptions, the principal radioimpurities are usually K, Th, and U. Complex production processes involving many stages and frequent contact with different reagents make it difficult to guarantee acceptable contamination levels. The

different chemical and physical behaviors of the elements of the U and Th decay series (Pb, Ra, Rn,...) sometimes result in deficiencies or isolated impurities of ^{230}Th/^{226}Ra, ^{210}Pb, and ^{228}Th and of their respective short-lived progenies. Other parent/daughter separations or equilibrium breakings are also possible but occur less frequently.

Only a few rules are in place that can help us judge the pathways of these contaminants along material fabrication. In metallurgy, the redox potential serves as a point of orientation. Thus the relatively high purity of copper can be explained by its high redox potential (0.337 V for the reaction $Cu \rightleftharpoons Cu^{2+} + 2e^-$ in acid solution) compared with K, U, and Th and with most of their daughter nuclides. Since Cu is routinely purified after smelting by electrolytical dissolution and redeposition in solution even in large-scale production, it is effectively separated from practically all radionuclides in the environment. The smelting of other base metals such as Sn or Pb usually involves the formation of a slag that consists mainly of iron silicates. This slag takes up the lithophile elements, i.e. elements that partition into the Earth's (siliceous) crust and not into its (metallic) core. Among these are the mineral-forming elements Si, Al, and O, as well as the alkali and earth-alkali elements and most transition elements. Thus, K (an alkali), as well as Th and U (actinides), are concentrated in the slag. If, however, Fe or even Al is to be produced, then more reducing conditions must be applied during smelting, which results in the dissolution of a larger fraction of lithophile elements in the metal phase. For the same reason the purification of these metals from Th and U and from their daughter nuclides is usually much more difficult to achieve, and special chemical separation processes (distillation of volatile components, phase separations in aqueous solutions, zone melting, etc) must be applied.

Plastic materials represent a completely different category; to discuss even a small fraction of the various substances that may be in use is impossible. As a general rule, one can assume that most plastics consist mainly of C, H, and O. Therefore, the major radioimpurities should be tritium and ^{14}C. However, most organic synthesis on an industrial scale starts from natural gas that contains very little tritium and ^{14}C. Despite this general expectation of radiopurity of plastics, one should be aware of the many possible contaminants that may derive from (inorganic) additives, catalysts, or mechanical engineering of hard plastics.

In general, distillation, crystallization, and above all zone melting are powerful purification methods by which to obtain radiopure materials.

The ongoing miniaturization of electronic circuits, especially of memory chips, with the growing risk of "soft errors" from α-particle radiation has stimulated the development of materials with low α-activity contamination. Consequently, Si and Ge are among the cleanest materials available at present. Their

radioimpurities are well below 10^{-12} g U/Th g^{-1} (3 μBq ^{232}Th kg^{-1} and 12 μBq ^{238}U kg^{-1}).

Moreover, Al that is normally strongly contaminated with U and Th (but depleted in $^{226/228}$Ra) can now be produced with less than 10^{-10}g U/Th g^{-1}. Production of modern lead with a low ^{210}Pb content ($\sim$ 0.4 Bq kg^{-1}) is also possible. These low levels of contamination were achieved by improving each production step under the surveillance of α-particle detection (30). For standard detectors such as gas, scintillation, or semiconductor counters, increasingly cleaner ingredients are becoming available. Typical background problems resulting from material and surface-related radioimpurities of these counters are addressed in Sections 4.2 and 5.

For cryogenic detectors with substances often not used previously in counting experiments, development is still in the initial phases. Electronic components such as resistors, capacitors, transistors, etc, need special attention if they are to be placed near the detector. Normally these components, even those used in hybrid or in Surface Mount Technology (SMT), are contaminated with K, Th, and U. Often ceramics are carriers of the contamination; individual pieces can contain up to several 10 mBq. Base plates for printed circuits should avoid glass fiber–reinforced materials since the latter may contain up to 20 Bq $\cdot$ kg^{-1} ^{226}Ra/^{228}Th/^{40}K.

We do not give here a complete list of potential radioactive construction materials. Some information can be found in the literature (27–29), and some is given in the body of this review. But experience teaches that because reliable information on these materials, on surface contamination, and on variations from batch to batch is lacking, the actual materials must be carefully tested prior to application. Ge spectrometry is the most powerful method for material selection, but other procedures are described in Section 4.2. Less problematic in this context are shielding materials.

2.2.1 SHIELDING MATERIALS Disregarding exotic elements such as tungsten or tantalum, a very limited number of materials are suited for the reduction of environmental γ rays, especially when cost is taken into account. Ideally, the material should have a high atomic number and low intrinsic activity. Hg, which is rather expensive, has a high radiopurity that can be even further enhanced by repeated distillation. Its longer-living radioisotope ^{194}Hg ($T_{1/2}$ = 520 years) is produced in noticeable quantities only by exposure to high-energy neutrons. However, Hg requires a container whose radiopurity is more difficult to control, which makes it less attractive. Fe is rather inexpensive but is usually contaminated through the monitoring of furnace linings with ^{60}Co. Old ship iron produced prior to the introduction of this procedure can be clean to below the mBq $\cdot$ kg^{-1} level (^{226}Ra, ^{228}Th, ^{40}K). Cu is least likely to be contaminated

by primordial radionuclides. However, like Fe, it has a rather high cross section for capture of thermal neutrons and for the cosmogenic production of radioactive nuclei. It is also inferior to higher Z materials such as Hg or Pb in the interaction with cosmic ray muons (Section 3.3). Pb is the ultimate shielding material because of its high atomic number, reasonable cost, and mechanical properties. Furthermore, it has a low neutron cross section and (see below) favorable low interaction probability with cosmic rays, including the formation of radionuclides by activation. Unfortunately, its intrinsic radioactivity is generally not negligible.

2.2.2 ^{210}PB IN LEAD The nature and origin of this contamination have been thoroughly studied by many authors and partially reviewed (31–35). The consistent overall result is that only ^{210}Pb with its daughter nuclides ^{210}Bi and ^{210}Po is responsible for the intrinsic radioactivity of lead. Owing to the long half-life of ^{210}Pb (22 years), the abundance of these nuclides in lead can be much higher than expected from secular equilibrium (36). The very soft β (E_{max} of 16.5 and 63 keV) and γ (46.5 keV) radiation of ^{210}Pb hardly escapes self-absorption, but the energetic (1.16-MeV) β rays of ^{210}Bi produce bremsstrahlung and characteristic X-rays in lead (see Figure 5 in Section 3.3). The bremsstrahlung continuum has its maximum at about 170 keV, while the lead X-rays have energies of 72.8, 75.0, 84.9, and 87.4 keV. ^{210}Po, the α-decaying member of this chain with an energy of 5.30 MeV, was recently found to diffuse to the surface of freshly scraped lead (37, 38). This diffusion results in an enhancement of the surface activity. Concentrations of ^{210}Pb reported in the literature range from the detection limit of the respective detector to 2500 Bq $\cdot$ kg^{-1} (39). In solder, where ^{210}Pb can also be introduced with the tin (40, 41), this contamination can be as high as 50,000 Bq $\cdot$ kg^{-1} (41). The contamination path of ^{210}Pb follows the uranium-containing minerals accompanying the lead ores. If these minerals are not completely separated at the beginning of lead production, their accumulated ^{210}Pb is taken up by the lead bullion during smelting. Added scrap lead already containing ^{210}Pb, or added antimony for hardening, or coal used in the reduction process can also result in contamination. Coal normally contains U in large quantities, from which ^{210}Pb is transferred to the smelting charge. Reduction processes without coal, such as electrically heated furnaces, prevent contamination via this pathway. Today, certified lead with specific ^{210}Pb activities of less than *(a)* 100 Bq $\cdot$ kg^{-1}, *(b)* 50 Bq $\cdot$ kg^{-1}, *(c)* 5 Bq $\cdot$ kg^{-1} and *(d)* 0.4 Bq $\cdot$ kg^{-1} is commercially available, e.g. from *(a)* Doe Run in the United States, *(b)* from Boliden in Sweden, *(c)* from Plombum in Poland) and *(d)* LC2 by Johnson and Matthey at a price only moderatly higher to about 100 times higher than that of regular lead. An alternative to certified lead is old lead produced several half-lives of ^{210}Pb ago. The availability of such lead, however, is

very limited, since "sources of supply" such as water pipes more than 200 years old, sunken shiploads, or ballast of sailing ships are rarely found. An exceptionally large load of antique Roman lead was recently discovered (42). Its ^{210}Pb content was measured with a bolometer and found to be less than 20 mBq $\cdot$ kg^{-1} (43), the lowest ^{210}Pb contamination in lead ever reported. Apart from ^{210}Pb and its progenies, no U or Th contaminations have been found so far in commercial lead. The most relevant upper limits measured for ^{226}Ra and ^{208}Tl are 0.25 and 0.29 (44) or 0.33 and 0.67 (45), respectively, all in mBq $\cdot$ kg^{-1}. The content of ^{40}K in LC2 lead (Johnson & Matthey) as measured by neutron activation analysis is about 0.3 mBq $\cdot$ kg^{-1} (E Pernicka, personal communication).

2.3 *Rn and its Progenies*

^{222}Rn, by far the strongest source of airborne radioactivity, is present in dwellings and laboratories at a concentration of about 40 Bq $\cdot$ m^{-3} on average. Consequently, 1 mm^3 of air contains about the same activity as that measured in solar neutrino experiments, for example. This comparison illustrates the importance of Rn as a background component and the demanding task of eliminating this component in such low-level experiments.

Admixtures of ^{220}Rn from the Th decay series vary strongly. This isotope's shorter half-life of 55.6 s (compared with 3.82 days for ^{222}Rn) makes its concentration more sensitive to barometric pressure changes and other factors influencing emanation. Although this isotope is present with about the same or higher activity levels in rocks, soil, and building material, its concentration in air is normally below the percent level of ^{222}Rn. ^{220}Rn presence strongly decreases with the distance from the emanating walls owing to its much smaller diffusion length during a lifetime. ^{219}Rn ($T_{1/2}$ = 3.96 s), a member of the actinium series, is negligible in most low-radioactivity background considerations.

Most importantly, the ^{220}Rn family dies out rather quickly, with a half-life of 11 h (^{212}Pb), but ^{222}Rn feeds into ^{210}Pb with a half-life of 22 years. The last γ-active nuclei for the ^{222}Rn chain is ^{214}Bi (neglecting here the 0.107% abundance of the 803.3-keV γ line of ^{206}Pb). Therefore, at least the γ activity of the ^{222}Rn family dies out with a half-life of 26.8 min (^{214}Pb) (see below). Short half-lives of ^{214}Po ($T_{1/2}$ = 162 μs) and of ^{212}Po ($T_{1/2}$ = 0.298 μs) are helpful in detecting very low ^{222}Rn/^{220}Rn concentrations using the delayed coincidences technique applied to the decay of mother and daughter.

The direct Rn progenies, originally positively charged, are in part attached to aerosols and in part form an unattached fraction (free atoms, ions, or ion clusters). Distribution depends strongly on the aerosol concentration. This distribution is important for health physic considerations (deposition in different parts of the respiratory tract) and therefore is covered in depth in the literature (46). It also plays a role in the so-called plate-out effect, i.e. the deposition

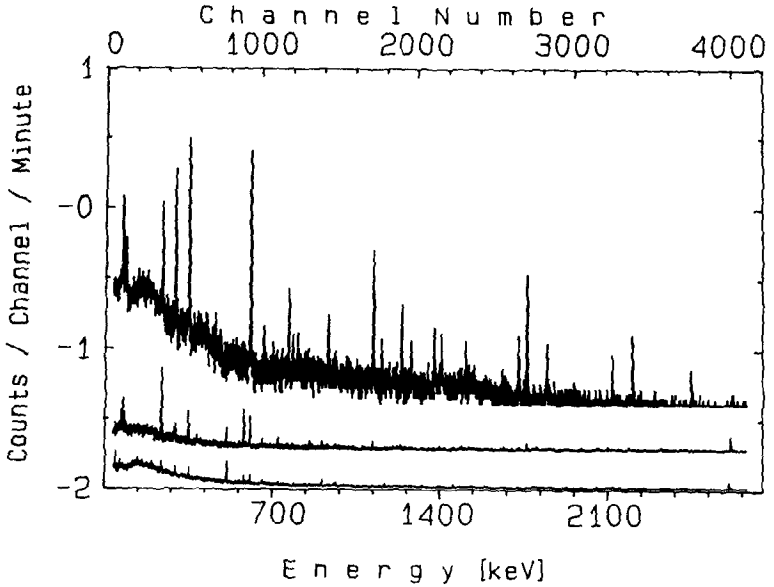

Figure 1 Ge-γ spectra of Rn progenies on a plastic foil at different time intervals after plate-out: the first 130 min (*top*); 200–1500 min (*middle*); 2–22 days (*bottom*). The spectra are shifted by constant values in order to avoid overlap from statistical fluctuations.

of the Rn progenies on surfaces. This effect is strongly enhanced on statically charged surfaces such as plastics or glass.

Figure 1 shows a dramatic example of the plate-out effect for a Ge spectrometer. Here, 0.5 m^2 of thin Kapton foil loaded with Rn progenies from the air were wrapped around the detector in several layers. The sample chamber was then evacuated, and spectra were recorded in different time intervals after plate-out (18, 47). The top spectrum (first 130 min) features mainly the lines of the ^{222}Rn family. The next spectrum (200–1500 min) is dominated, although less strongly, by ^{212}Pb and ^{208}Tl, the ^{220}Rn daughters. Finally, at the bottom, we have the background spectrum of the detector without contribution from Rn. If the sample chamber is not evacuated, a third component appears: ^{214}Pb and ^{214}Bi, decaying by the half-life of ^{222}Rn. The ^{210}Pb activity reduced by the half-life ratio of 3.82 days to 22 years is not detectable here. However, accumulated over long periods it may disturb other experiments, in particular those that are sensitive to the α particles of its daughter, ^{210}Po.

Cleaning procedures for plated-out Rn progenies on plastics have been tested (M Deutsch, private communication). The best results were obtained with acid

leaching. Hot 70% nitric acid removed up to 99% of ^{212}Pb, up to 97% of ^{214}Pb, and up to 90% of ^{210}Pb. The remaining residue was probably embedded by recoil. A small fraction of Rn had also diffused into the plastic, which in the end also results in an unremovable ^{210}Pb fraction. In shorter-term experiments, memory effects of back-diffused Rn must be considered.

The best way to protect a detection system against Rn and its strong concentration variation in air (48, 49) is to encase the system with metal foil or a metal sheet as tightly as possible (50). A small overpressure of old compressed air, of N from a steel cylinder, or of evaporated N from a liquid N reservoir can help expel enclosed Rn and suppress influx through cracks or small openings.

If plastic foil is used as a barrier, its permeability to Rn must be taken into account. The permeability P is the product of the diffusion coefficient D and the solubility S, i.e. $P = D \cdot S$. Both P and D are strongly dependent on the molecular (polymerization) structure of the plastic. At 25°C, P ranges from about $5 \cdot 10^{-5}$ cm^{2}s^{-1} for silicon rubber to about $1 \cdot 10^{-10}$ cm^{2}s^{-1} for nylon (51, 52). The equilibrium concentration of Rn (c) on the inside of a plastic foil isolation (if $c_a \gg c$) is given by $c = FPc_a(Vd\lambda)^{-1}$, where F is the surface area of the foil, c_a is the radon concentration in air, V is the gas volume inside the foil, d = thickness of the foil, and λ is the decay constant of Rn. Overpressure on the inside of the foil with Rn-free gas cannot prevent diffusion because the latter depends only on *partial* pressure differential. Other Rn suppression techniques in low-level counting are discussed in Reference 50.

Rn is highly soluable in water and even more so in organic solvents. At room temperature (18°C), 0.285 cm^3 of ^{222}Rn are dissolved in 1 cm^3 of H_2O, and 12.8 cm^3 are dissolved in 1 cm^3 of Benzene (at 1 atm partial pressure of ^{222}Rn) (53). Experiments using water as a detector or as a shield need to deal with starting concentrations that can reach 100 Bq ^{222}Rn l^{-1}. Possible methods of reduction include flushing with nitrogen and vacuum extraction.

3. COSMIC RAY-INDUCED BACKGROUND

Primary cosmic ray particles (about 90% protons, 9% α particles, and 1% heavier particles) hit the earth atmosphere at a rate of about 1000 m^{-2}s^{-1} (54). Their interaction with atmospheric atoms generates the following variety of elementary particles (listed in approximate order of intensity): neutrons, electrons, neutrinos, protons, muons, and pions. The total intensity of these secondaries reaches a maximum at an atmospheric depth of about 150 g/cm^2(13.7 km altitude) and then falls off gradually, with the nucleons experiencing the sharpest decline. At sea level, the relative intensity of charged pions:protons:electrons:neutrons:muons is about 1:13:340:480:1420, with

$1.34 \cdot 10^{-5}$ $cm^{-2}s^{-1}$ for charged pions (20). These fluxes are dependent on the geomagnetic latitude and on the phase in the 11-year solar cycle. The flux fluctuations are quite large, especially for neutrons. The continuous interplay of absorption and new formation in the measuring device is not easy to control. More data on cosmic ray secondaries can be found in the compilation of Allkofer & Grieder (55). For additional information on cosmic rays in general we refer the reader to Gaisser (56).

Only muons and neutrons are relevant particles in low-radioactivity background techniques. Electrons and photons (historical term: weak component) as well as protons are directly absorbed by the Pb shield or by overburden from building ceilings. However, protons and charged pions contribute to the production of cosmogenic nuclides in the first few 10 $g \cdot cm^{-2}$ of material below rock surface.

Neutrons are attenuated with a mean length of about 200 $g \cdot cm^{-2}$ (57), mainly via inelastic scattering. Muons, on the other hand, lose their energy in standard rock on a much longer scale (about 2 $kg \cdot cm^{-2}$ near sea level) by ionization, pair production, bremsstrahlung, and nuclear interaction (58). Because of the energy-range relation, the differential spectrum of muons is shifted to higher energies with growing underground depth (59).

Figure 2 shows in a qualitative way the flux of muons and of secondary neutrons (nucleonic component) for shallow depth (18, 60). In addition, the production of tertiary neutrons by muons in a typical Pb shield is indicated, as is the flux of neutrons originating from natural fission and from (α, n) reactions for U and Th concentrations of the continental upper crust [36 Bq ^{238}U kg^{-1}, 44 Bq ^{232}Th kg^{-1} (20)]. In high Z material, the neutron production via capture of negative muons, photonuclear reactions, and photofission of real and virtual photons associated with fast muons is strongly enhanced. Therefore, tertiary neutrons dominate in a massive Pb shield already below a few meters of water equivalent (m.w.e.). Fission and (α, n)-derived neutrons become important only below a few 100 m.w.e.

3.1 *Radioisotope Production*

Secondary cosmic ray particles generate background not only directly via interactions in or near a detector but also indirectly through the production of radionuclides. Particularly at sea level and even more during transport in air, the activation by the hadronic component can reach specific radioactivity levels higher than the residual contamination from primordial nuclides. In $\beta\beta$ decay experiments based on Ge diodes, cosmogenic radionuclides produced above ground dominate the background at the beginning of the underground operation (44, 61–63). Radiochemical solar neutrino experiments can only be performed deep underground, since side reactions from cosmic ray secondaries

leading to the same isotope as neutrino capture are higher by many orders of magnitude at sea level.

The study of cosmogenic production has its roots in meteoritic and lunar research, which has led to a profound understanding of production rates and has stimulated an extended compilation of cross sections needed to estimate these rates (64). Terrestrial in situ cosmogenic studies began two decades later, primarily because the required sensitivity is three to four orders of magnitude higher (24, 65). For comparison, the mean specific activity (equivalent to the production rate if in equilibrium) of ^{26}Al in meteorites is 1 Bq $\cdot$ kg^{-1} (or 1 atom kg^{-1}s^{-1}) and 1 mBq $\cdot$ kg^{-1} in Si at sea level.

Longer-living radionuclides such as ^{26}Al, ^{10}Be, and ^{36}Cl, which are accessible to accelerator mass spectrometry or stable nuclides, e.g. ^{3}He, are of primary interest in earth sciences such as geomorphology, archaeology, glaciology, and oceanography. Their production rates have also been investigated as a function of shielding depth (24, 65).

In low-level experiments, however, the cosmogenic background component is caused by shorter-living radionuclides (e.g. $^{56-58}$Co, ^{60}Co) produced primarily in other target elements. Closer to the targets of our interest, which

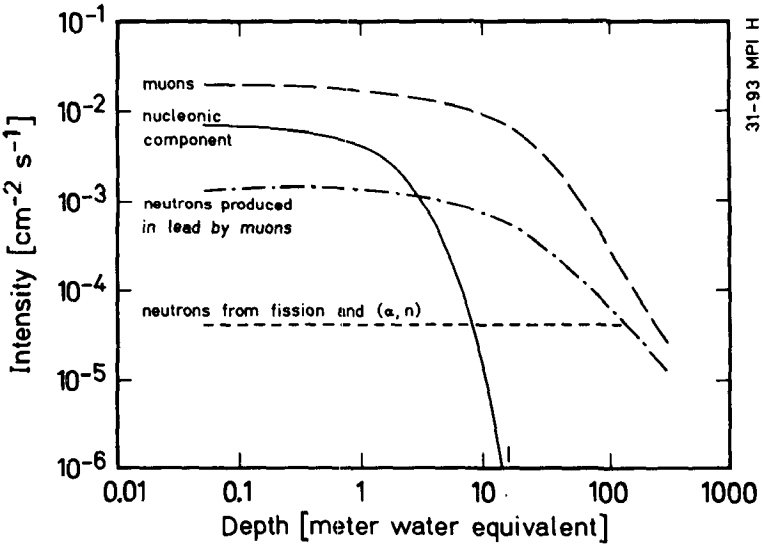

Figure 2 Flux of cosmic ray secondaries and tertiary-produced neutrons in a typical Pb shield vs shielding depth. Neutron flux from natural fission and (α, n) reactions is also shown. The nucleonic component is more than 97% neutrons.

Table 1 Measured cosmogenic production rates (saturation activity) in natural and enriched germanium

	Production rate (μBq kg^{-1})		
		Enriched[a] germanium (69)	
Isotope	Natural germanium (68) (sea level)	sea level	~11 km
^{54}Mn	38 ± 9	27	$4 \cdot 10^3$
^{57}Co	34 ± 5	19	$6 \cdot 10^3$
^{58}Co	40 ± 10	14	
^{65}Zn	440 ± 70	127	$3 \cdot 10^3$
^{67}Ga	610 ± 170		
^{68}Ge	350 ± 80		

[a]86% ^{76}Ge, 14% ^{74}Ge

include detector or construction materials such as Ge or Cu, are production rate calculations for space experiments (66). These calculations are for the most part based on the model of Silberberg & Tsao (67) for spallation reactions. The lack of real measurements and calculations (68–70) in our field may be compensated by combining information from the terrestrial and space estimation approach. Table 1 summarizes measured production rates in natural and isotopically enriched Ge. Small differences in altitude or in coverage by building structures strongly influence these rates; hence comparisons are difficult if the exposure conditions are not identical. The strongly enhanced rate at high altitude (Table 1) produces in a 10-h flight about the same activity as that observed after 125 days of exposure at sea level. Consequently, air transportation of material or equipment is a risk in highly sensitive experiments (e.g. ^{76}Ge $\beta\beta$).

As an example of underground cosmic ray production, Figure 3 shows the dependence of ^{71}Ge induced in $GaCl_3$ as a function of depth (71). This dependence was derived from measurements and calculations (72) for the Cl detector and from a measured cross-section ratio of ^{37}Ar from C_2Cl_4 and of ^{71}Ge from $GaCl_3$. Like the fluxes in Figure 2, the production rate here is also dominated by the nucleonic (neutron) component at shallow depth and by fast muons below about 10 m.w.e. The solar neutrino capture rate of approximately 1 atom day^{-1} corresponds to the muonic signal at 500 m.w.e. In order to keep this rate a small fraction of the solar signal, a much deeper location is required.

In nuclear transformation of the type $Z \rightarrow Z-1$ the contribution of stopped negative muons is stronger than in the example shown in Figure. 3. Often it dominates at shallow depth the nucleonic production. Its production rate R is given by $R = I_\mu P_c P_e$, where I_μ is the stopping rate of negative muons, P_c is the

capture probability in the target nuclei, and P_e is the emission probability for the number of neutrons, as that the isotope of interest is produced. P_c increases strongly with Z, and P_e is at maximum if one neutron is emitted.

Fast muons produce energetic particle showers of protons, neutrons, and π mesons that can extend over several cubic meters of volume, predominantly in the forward detection. In this cascade the production rate is strongly enhanced by secondary reactions.

Details on μ^- capture are provided by Singer (73). Stopping rates of negative muons have been evaluated by Bilokon et al (74) and by Charalambus (75); for capture rates see Reference 76. Estimates of nuclear disintegrations due to neutrons, fast muons, and capture of negative muons are given by Lal (24). Underground production of some radionuclides via neutrons from muon

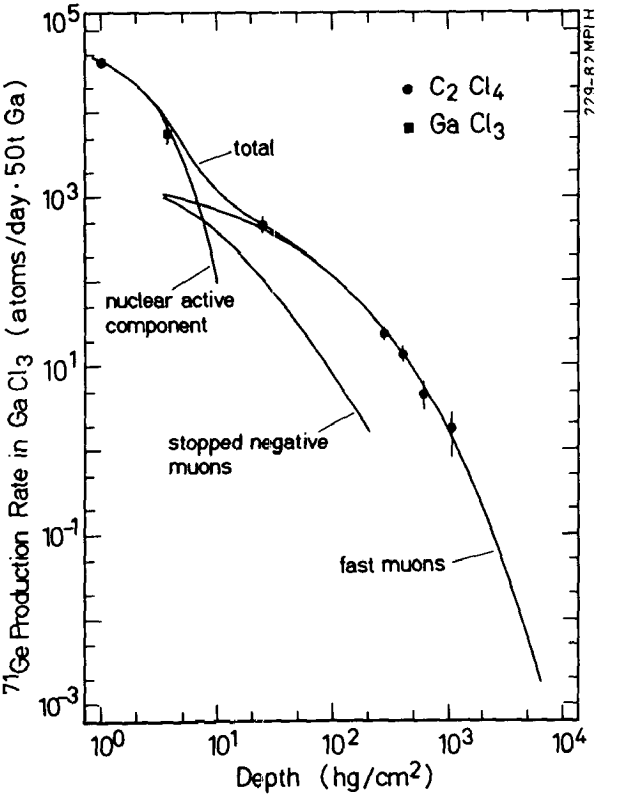

Figure 3 Cosmic ray production of ^{71}Ge in $GaCl_3$ vs shielding depth.

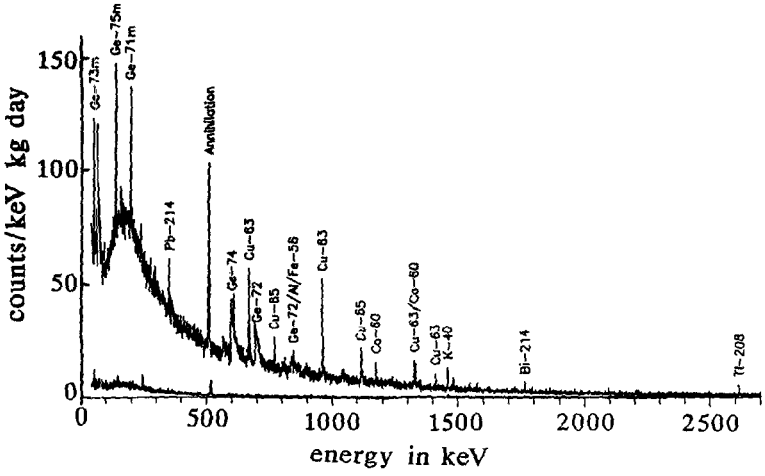

Figure 4 Background spectra of similar Ge spectrometers (0.9 kg active volume) with passive and active shielding at sea level (*top*) and at 15 m.w.e. (*bottom*).

reactions, (α, n) reactions, and natural fission has been covered by Florkowski et al (77).

3.2 *Neutron-Induced Background*

Inelastic scattering and radiative capture are the main channels for direct neutron-induced background. In dark matter experiments searching for WIMPs, the nuclear recoil can be faked by neutrons. Sufficiently energetic neutrons and WIMPs both scatter elastically from a nucleus in the detector, then neutrons have the same signal signature and cannot be differentiated.

In Figure 4, spectra of shielded Ge detectors at sea level (78) and below 15 m.w.e. (79) are compared. In both cases, Cu is used as inner shield lining, and the muonic component is reduced with veto shields consisting of three flat multiwire proportional chambers in the upper (sea level) spectrum and six in the lower (below 15 m.w.e.) spectrum. The upper spectrum is clearly dominated by neutron-induced lines. These lines can be attributed to inelastic scattering and to (thermal) neutron capture in Ge or in the cladding and lining material. The absence or low intensity of these lines in the lower spectrum indicates that, at 15 m.w.e., secondary neutrons are well filtered out. As shown in Figure 2, tertiary neutrons dominate in this case, but since the veto detector is highly sensitive to the (neutron-producing) muons, tertiary neutron-induced lines are suppressed, provided their lifetime is in the range of the veto blocking

time. The proportional gas chambers have only a small detection efficiency for neutrons. From the ratio of the line intensities, the neutron flux is reduced by a factor of 10 to 15. Differences in the spectral distribution of the neutrons also exist. Tertiary neutrons have an evaporation-type spectrum and a high-energy component, largely as a result of μ capture at this depth (80). They therefore have a lower thermal fraction than secondary neutrons upground, which can be attributed to the absence of low Z-moderating material in the shield. The difference in the continuum of both spectra is due not only to the reduced neutron flux but also in part to a less effective veto and a higher contamination level in the spectrometer at sea level.

A compilation of lines from neutrons, muons, and activation observed in Ge-γ spectrometry is given in Table 2 of Reference 18 and in Table 1 of Reference 81. In these references, the relative count rates of these lines are partly discussed and line shape peculiarities such as the broadening by the recoil of the producing neutron (82; see also Figure 4) are described.

The usefulness of an additional neutron absorber in the shield (best borated polyethylene, PE) depends on the type of experiment and its overhead shielding. To effectively absorb tertiary neutrons, the absorber should be positioned inside the lead. However, this positioning results in an enlarged target mass for muon interaction and a cubic increase in cost. Figure 2 provides here some guidance. To appreciably reduce the nucleonic component at sea level, the neutron absorber must be rather thick, even though paraffin or PE has a shorter attenuation length than soil or rock. A veto that is also sensitive to neutrons, e.g. a plastic or liquid scintillator, might be a superior solution. More systematic investigations are clearly needed.

An outside veto shield with a high registration probability for the producing muons is effective in the background suppression of neutron events, at least for Ge spectrometers at shallow depth with predominantly tertiary neutrons (see above). The background contribution from neutron-induced radioisotopes with half-lives exceeding the veto time is rather small, although not negligible for extremely sensitive experiments (18). If no moderator is present, tertiary neutrons may escape from the shield before inducing a background event. The average time required for a fast neutron to become thermalized and to be captured in lead is about 900 μs. In a moderator substance, however, this time is much shorter. Only at deep locations, where the neutron flux is dominated by fission and (α, n) reactions, is a neutron shield, if needed, best placed outside.

In WIMP search, background due to neutrons is much more severe. The cryogenic detection technique, which is well suited for this task, is still in the test phase and is therefore developed preferentially near the home laboratory

at shallow depth. Neutron measurements (83) with a moderated BF_3 proportional counter have shown that in the Stanford Underground Facility (17 m.w.e.), 25 cm of moderator inside a 10-cm-thick Pb shield reduced the neutron flux from $(1.04 \pm 0.04) \cdot 10^{-3}$ cm^{-2}s^{-1} to $(7.1 \pm 2.0) \cdot 10^{-6}$ cm^{-2}s^{-1}. The first number (flux in lead without moderator) is in good agreement with the tertiary flux given in Figure 2. In the facility itself, the flux was $(8.1 \pm 0.6) \cdot 10^{-5}$ neutrons cm^{-2}s^{-1}; consequently, tertiary production has enhanced the neutron flux in the Pb shield by a factor of about 13. The neutron flux in the facility, together with that of other locations, is listed in Table 2.

The flux measured at Gran Sasso (Table 2, 3400 m.w.e.) originates only from (α, n) reactions and ^{238}U fission. A rough estimate of the muon-produced fraction that makes use of the neutron production rate per muon vs depth relation given by Aglietta et al (89) yields a flux from this source about three orders of magnitude lower than that from natural activity. More underground neutron measurements and estimates from the (α, n) and fission source are provided by Florkowski et al (77). Thick-target (α, n) reactions have been studied by Heaton et al (90).

Table 2 Measured neutron fluxes at different altitudes and in underground laboratories

Location	Energy	Flux ($\times 10^{-6}$ cm^{-2}s^{-1})	Reference
3195 m	0.4 eV–0.1 MeV	38000	84
	0.1–1 MeV	19000	
	1–10 MeV	17000	
~1000 m	0.025–0.3 eV	1400	88
	0.3–500 eV	6900	
	0.5–10 MeV	5700	
Sea level	total	4000	86
	0.4 eV–0.1 MeV	2900	84
	0.1–1 MeV	1600	
	1–10 MeV	1700	
17 m.w.e.	total	81 ± 6	83
	11.5–50 MeV	$1.07^{+0.41}_{-0.30}$	85
3400 m.w.e.	thermal	1.08 ± 0.02	87
	0.05 eV–1 keV	1.98 ± 0.05	
	> 2.5 MeV	0.23 ± 0.07	
	0.025–0.3 eV	2.05 ± 0.06	88
	0.3–500 eV	1.28 ± 0.31	
	1.5–10 MeV	2.56 ± 0.27	

3.3 *Muon-Induced Background*

The indirect background contribution from muons via activation and neutron production has already been discussed in Sections 3.1 and 3.2. We concentrate here on the direct interaction of muons.

Muons are decelerated almost exclusively by electromagnetic interaction with the traversed matter. This deceleration results in high-energy electron/positron/photon showers from δ electrons (knock-on electrons), direct electron pair production, and muon bremsstrahlung. The energy loss occurs in very small fractions of the primary energy. In combination with the relativistically extended decay length, this low loss rate allows muons to penetrate deep into the earth crust. While at rest, muons either decay or, in case of negative muons, may be captured by a nucleus. In the former case, another shower follows from the decay electron. In the latter case, the Z of the target nucleus is reduced by one unit; one or several neutrons are emitted; and some MeV remain for excitation (shower production).

The electromagnetic interaction (mainly ionization) results in a high specific energy deposition in the detector upon direct hits. Depending on the energy, between 1 and 6 MeV are deposited per $g \cdot cm^{-2}$ in NaI(Tl) or Ge detectors (78). The spectra of Ge detectors from direct muon hits and from showers of muon-generated electrons in neighboring materials have been simulated by various authors (78, 91–93).

In Figure 5, the effect of the shower bremsstrahlung for different inner shield linings is compared with bremsstrahlung from ^{210}Bi in lead (18, 81). The vetoed spectra of both upper cases are depicted in the same frame. For the ^{210}Bi (^{210}Pb) measurement, the veto was also active. The spectral differences in Fe (*top*) and Pb (*middle*) can be explained by self-absorption of bremsstrahlung photons in these linings. The similarity (up to 500 keV) between the two lower spectra indicates that 1 muon $cm^{-2}s^{-1}$ results in the same integral count rate (100–500 keV) as 7 kBq ^{210}Pb kg^{-1}. For the X-ray intensities the corresponding equivalent is 2.4 kBq ^{210}Pb kg^{-1} (18, 81). When a shield for shallow depth is designed, these values will be important in choosing a sensible level of ^{210}Pb purity for the inner lead lining (see below). The annihilation line in the upper and middle spectrum is due to shower pair production and to decaying μ^+.

Depth-intensity relations for muons have been given by Crouch (94) and Gaisser (56) and can also be found in the general compilation on cosmic ray secondaries of Allkofer & Grieder (55).

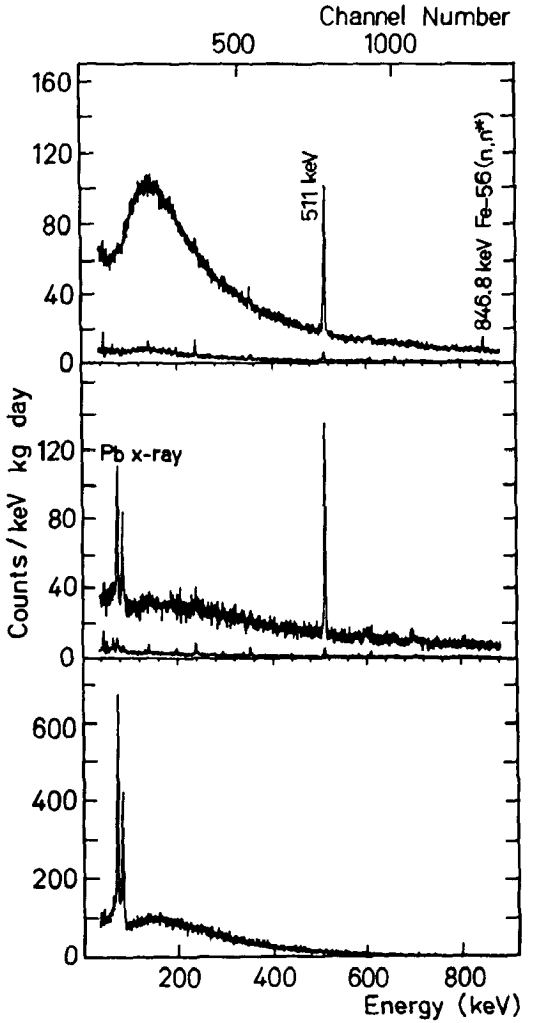

Figure 5 Background spectra of a germanium detector (0.9 kg active volume) at 15 m.w.e. with 5-cm-thick different inner-shield lining: old ship iron with and without veto (*top*), low-activity lead—0.4 Bq ^{210}Pb kg^{-1}.—with and without veto (*middle*), and lead containing 130 Bq ^{210}Pb kg^{-1} (*bottom*).

4. BACKGROUND SUPPRESSION METHODS

4.1 *Shielding*

In light of the above discussion on radioimpurities and cosmic ray interaction, the ideal shield against external γ rays for an installation at sea level would consist of low-activity Pb. Since lead with a low ^{210}Pb concentration is normally more expensive than regular lead, a shell-like construction with decreasing ^{210}Pb content toward the detector would be most economic. Pb seems to be superior to other shielding materials in regard to its background interference resulting from the interaction of neutrons and muons and from activation.

A shield thickness of between 10 and 15 cm is sufficient if no cosmic veto shield is used. Beyond that thickness, muonic-induced bremsstrahlung, together with a smaller contribution from secondary neutrons, dominates the background spectrum. Both cannot be significantly further reduced with more lead (18). In this discussion, we presume that there is no direct line of sight to the environment. Figure 6 shows the shielding effect of 15 cm of lead for a germanium detector at sea level and at about 500 m.w.e. (95). The middle spectrum is composed of only neutron-induced lines, the muon-induced annihilation

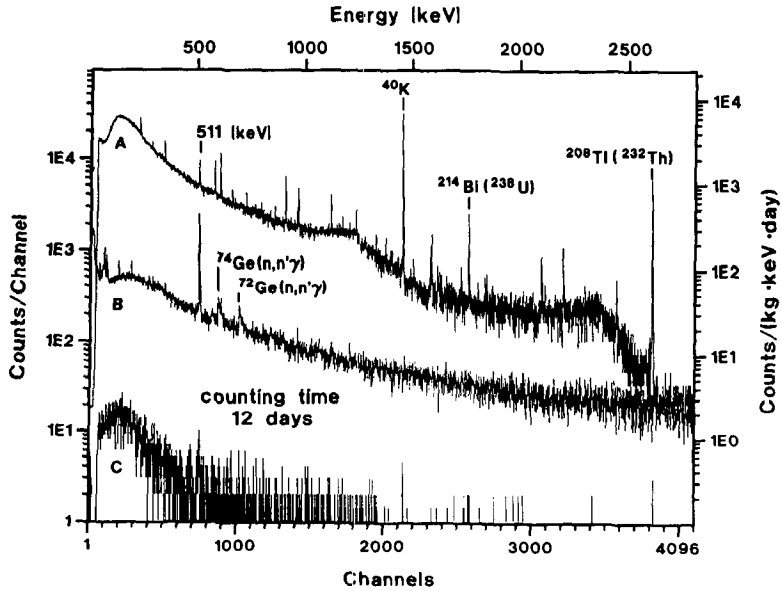

Figure 6 Background spectra of a Ge detector (0.5 kg active volume) without shield (*top*), with 15-cm lead shield (*middle*), and with the same shield at about 500 m.w.e. (*bottom*) (95).

line, and the bremsstrahlung continuum from muonic secondary electrons. The full photon attenuation of the lead shield is only effective at the deep location. It is mainly determined by the most energetic natural γ line, which is that of ^{208}Tl with 2.615 MeV. When passing through the lead, lower-energy photons are continuously replenished by Compton scattering of the higher-energy photons such that the continuous spectrum reaches an equilibrium shape. Figure 6 does not clearly show this effect in the lower spectrum because of low statistic. The higher count rate at low energies is probably caused by ^{210}Pb or by another β-active contamination near the crystal. Shizuma et al (96) have also studied the optimum lead thickness. The usefulness of additional neutron absorption in the shield was discussed in Section 3.2.

A Monte Carlo simulation tailored to a Ge detector at 15 m.w.e. revealed that 99% of all ^{210}Bi events observed with the detector originate from the inside 2 cm of lead facing the detector (A Müller, personal communication). This result gives an idea of the required thickness of the innermost lead shell. This shell's acceptable level of ^{210}Pb contamination depends on the muon flux in the laboratory and on whether a veto shield is used. The integral count rate (100–500 keV) induced by muons would correspond to about 140 Bq^{210}Pb kg^{-1} for a spectrometer at sea level and to about 50 Bq ^{210}Pb kg^{-1} for the lead X-ray count rate (see Section 3.3). An inner lining with material of lower Z is recommended only if X-rays of the adjacent material have to be absorbed (81).

At still lower net muon fluxes due either to more efficient veto counters or to larger depth, electrolytic Cu is superior as an inner shielding material. Its higher radiopurity balances the lower self-absorbtion for bremsstrahlung induced by muonic secondary electrons. The suppression of Rn must also be taken into account when designing a shield. Some recommendations in that direction have been given above (see Section 2.3).

4.2 *Radioassay Techniques and Material Treatment*

Material selection is the most fundamental prerequisite in low-radioactivity experiments. In this respect, nondestructive γ spectrometry with Ge detectors is the most powerful screening technique. This technique is sensitive to all types of radiation that are not directly self-absorbed in the investigated material. β particles, e.g. of ^{210}Pb/^{210}Bi, are also detectable if their energy exceeds a few 100 keV. However, since β detection in Pb, Sn, Mg, etc, is mediated primarily via bremsstrahlung or X rays, the sensitivity is strongly reduced compared with direct γ counting.

The most prominent contaminants, ^{40}K, ^{232}Th, and ^{238}U, are detectable at mBq $\cdot$ kg^{-1} levels and lower, corresponding to 10^{-10} g g^{-1} for U and Th and to 10^{-8} g g^{-1} for K. Low background and large sample capacities allow reasonable counting times (47, 97). Within certain limits, deviations from secular equilib-

rium can also be observed. Although NaI(Tl) detectors are available in larger sizes, their higher efficiency cannot compete with the high diagnostic power of Ge diodes because of their inferior energy resolution. The higher achievable radiopurity is another advantage of Ge detectors relative to scintillation detectors. Photomultipliers cannot yet be obtained without substantial contamination of the isotopes under discussion. Photodiode readout is a promising alternative under development. An organic scintillation can compete only when coincidence techniques in the detection of positron emitters or of radionuclides with cascading γ decay are applied. Here and in the methods discussed below the universal sensitivity to radioactivity as offered by Ge-spectrometry is no longer fulfilled. Additional methods by which to measure these primordial nuclides are α counting, neutron activation analysis (NAA), and various types of mass spectrometry.

Modern α spectrometry with silicon detectors yields high-energy resolution and, as a result, a low background [some counts per day (cpd) in the natural α lines]. The sensitivity is limited by the thin (less than 0.5 μm) source layer required to maintain the good energy resolution. This technique and the chemical extraction procedure result in sensitivity ranges of 1–100 mBq kg^{-1} for U and Th. The same applies for the α-emitting progenies such as ^{210}Po, which is used for ^{210}Pb measurement in lead (detection limit 100 mBq kg^{-1}; M Wojcik, personal communication). Only α spectrometry provides a quantitative analysis of the U and Th isotopes.

The NAA sensitivity of 10^{-12}–10^{-10} g g^{-1} for U, Th, and K depends strongly on the matrix of the sample to be analyzed. With low-level Ge spectrometry and large (>1 g) sample radiochemistry, 10^{-13} g g^{-1} is attainable in special cases. Conventional (thermal ionization) mass spectrometry typically reaches 10^{-12}g g^{-1} for U and Th, and a value of about 10^{-14}g U g^{-1} and 10^{-13}g Th g^{-1} is possible with inductively coupled plasma mass spectrometry (ICPMS). Accelerator mass spectrometry (AMS) is approaching this sensitivy range as well (98).

^{226}Ra needs special attention since it is often separated from the U chain. Its most sensitive measurement is via ^{222}Rn, which is extracted from any large quantity of material, collected on charcoal, and measured in various types of Rn detectors, e.g. a Lucas cell [a ZnS(Ag) coated cell viewed by a photomultiplier], gas counter, slow or fast ionization chamber, liquid scintillation, or solid-state α counter. The miniature proportional counter developed for radiochemical solar neutrino experiments (99, 100) allows us to measure as little as 200 μBq of Rn with reasonable statistics (10%). Only the blank rate (signal of the detection system without a sample) from the extraction and concentration apparatus limits this analytical method for Ra and Rn. Almost equally high sensitivity is attained with miniature Lucas cells developed for ^{222}Rn detection in the Sudbury Neutrino Observatory (SNO) (101).

The above-mentioned counting methods are routinely used for Rn monitoring in air. The highest sensitivity for direct Rn counting (without preconcentration) is achieved by collecting the charged progenies with a high-voltage field onto the surface of a thin α counter in a large-volume chamber (J Postendörfer & A Reineking, personal communication; 102). Concentrations as low as 100 mBq ^{222}Rn m^{-3} can be monitored in this way. In addition, ^{222}Rn and ^{220}Rn can be separated. Slow ionization chambers that have an active volume of several liters might be effective in this context as well (B Kromer, personal communication). A large scintillation chamber working in the coincidence mode almost matches the same sensitivity; however, it cannot distinguish ^{222}Rn from ^{220}Rn (103).

Low-energy contaminants such as ^{3}H and ^{14}C are generally measured with liquid scintillation counting (LSC). As in other methods dependent on photon counting, the background is determined by the primordial contamination in the phototube. The move toward low-background counting in LSC recently began with the introduction of veto and coincidence techniques (104). The sensitivity of commercial LSC counting ranges from mBq to Bq l^{-1} ($8 \cdot 10^{-11}$ to $8 \cdot 10^{-8}$ g U g^{-1}). A solar neutrino experiment based on liquid scintillation (Borexino) is present only in the test phase. This experiment needs to push the radiopurity of the scintillator below 10^{-15}g U/Th g^{-1} and 10^{-14}g K g^{-1} (105; see also Section 5.1) and thus many orders of magnitude beyond previously faced levels.

Gas counting has the longest tradition not only in ^{3}H and ^{14}C measurement but also in low-level counting in general (106, 107). Its sensitivity exceeds that of LSC. Today, ^{14}C is measured primarily with AMS. Low specific concentrations of rare gas radionuclides (e.g. ^{37,39}Ar) are best detected with high-pressure proportional counters (108).

4.2.1 MATERIAL TREATMENT Surface-related contamination requires special attention during the assembly of low-background spectrometers. Acid cleaning with appropriate chemicals under clean-room conditions has proved effective. The radiopurity of the acid seems to be less important as long as the final cleaning step is performed with ultrapure water. In a systematic study of the leaching of trace elements from plastics, this was also found to be the case (109). Because HCl and HNO_3 appear to leach various elements with different efficiencies, the use of both acids, one after the other, is recommended.

If lye has to be used for some metals (e.g. Al) or semiconductors (e.g. Si), it should be free of K. For the latter, a mixture of HF and HNO_3 is preferable. Electropolishing is effective for surfaces of Cu, Fe, and Ni as well as for their alloys. This method is widely applied in high-purity chemical processing plants. Special recipes for the polishing liquids do not always guarantee their radiopurity, but here again the final passivation and rinsing step is the determining factor. In contrast to normal acid cleaning, electropolishing smoothes

the surface. This treatment reduces the likelihood of recontamination since the deposition probability for particulate is lowered. In addition, the reduced surface area helps lower Rn emission through α recoil from near-surface Ra contamination and accelerates degassing in vacuum applications.

Some joining techniques, such as normal welding or soldering, may result in strong contaminations of the material with primordials from the jacket of the welding rod or with ^{210}Pb from the solder. Inert-gas TIC welding and hard soldering with solder with a high Ag concentration, both of which are used in high vacuum techniques, are less problematic, but electrobeam welding is superior. An acceptable compromise is to glue joints with cyanacrylat. A special warning is given for electrolytic (gold) plating because it can incorporate K, which is present in the electrolysis bath.

Electroforming of copper parts can produce complicated parts that are free from primordials (110). Because this process removes nonelemental impurities in general, it also helps reduce cosmic radioisotopes, e.g. $^{56-60}$Co accumulated during upground storage.

Proportional counters are most sensitive to contamination of the inner surface. Loosli et al (111) have studied its relative background contribution as well as other sources. Low-level gas counting in general is reviewed by Povinec (106).

4.3 *Active Background Discrimination Techniques*

The background rejection of penetrating muons with anticoincidence detectors is widely applied. Other discrimination techniques use decay sequences (coincidence), signal patterns (rise time), or multiple detection mechanisms (e.g. ionization-scintillation) to distinguish signal from background. In dark matter search, different signal combinations of the last type are being tested or envisioned, e.g. heat (phonons) and ionization, heat and scintillation, scintillation and scintillation (in different spectral ranges or primary and secondary), etc. These combinations are helpful in electron-recoil/nuclear-recoil discrimination in various bolometer types, in cooled NaI and in liquid Xe.

All these discrimination techniques need some cuts in the acceptance windows since their signal distributions do not form sharp lines and partly overlap. We therefore must accept losses in detection probability. Some of these techniques are outlined in the description of individual experiments (see Section 5).

4.3.1 VETO AND COINCIDENCE TECHNIQUES A veto counter device should encapsulate the shield or detector array as completely as possible without dead edges (see e.g. 97, 112). The device described in Reference 112 was constructed for another type of experiment but serves the same purpose. With growing overburden, the angle distribution of muons (about $\cos \delta^2$ at sea level, δ azimuth angel) grows steeper so that at very deep locations, a top counter

suffices. The veto efficiency is best estimated from the suppression of the direct muon interaction peak at about 40 MeV for a 1-kg Ge crystal. At this high energy range, no other background contributes.

Scintillator veto detectors are more effective at sea level and shallow depth than gas counters (see Section 3.2). They also help reduce background events induced by secondary neutrons (97, 113, 114). In order to keep the count rate of the scintillator at a rate that allows longer veto times (> a few μs) an additional layer of lead should be used to shield against environmental γ radiation (114).

Large NaI(Tl) multidimensional systems with veto or Compton suppression systems made of either NaI(Tl) (115) or plastic scintillator (116) have been extensively used in the past. Multicoincidence measurements are very selective for nuclides undergoing positron decay or cascade decay. In general, their veto has a larger suppression factor for cosmic events compared with those from radioactive background since muon-induced showers have a high multiplicity. Ge-NaI(Tl) combinations also found wide application (45, 117–119). Typically, as for most experiments with scintillators, their background was limited by the contamination of the photomultiplier (glass) with primordials.

A state-of-the-art Compton suppression Ge-NaI(Tl) spectrometer has been constructed for the Lawrence Berkeley Laboratory (LBL)/University of California at Santa Barbara (UCSB) ^{76}Ge $\beta\beta$ decay experiment (120). This spectrometer was operated in the Oroville Dam about 600 m.w.e. underground. Up to eight 0.9-kg Ge detectors were mounted inside a cavity formed by 10 blocks of 15-cm-thick NaI(Tl), thus providing an active veto with a threshold of 30 keV. The cryostat was comprised of electroformed copper of only 0.25-mm wall thickness so as to achieve high radiopurity and an effective Compton suppression. The anti-Compton veto cancels not only muon-induced events but also (in most cases) scattered photons that exit from the Ge crystal and any other time-coincident event that had triggered the NaI(Tl). The background in the $\beta\beta0\nu$ region of ^{76}Ge (around 2038.6 keV) was with 0.3 counts (keV $\cdot$ kg $\cdot$ year)$^{-1}$ (121), comparable to passively shielded Ge detectors (44, 122). However, peak count rates for the U and Th series were high compared with the latter ones, despite the high suppression probability for these mostly cascading gamma lines. This excess again originates from the primordial contamination of the photomultiplier tubes (PMTs).

Here, as in any other deep underground low-radioactivity experiment, the question arises as to whether an active shield or a purely passive shield is superior for background improvement. In general, one would assume that as long as an active shield is less radiopure than both the detector and the passive shield, then the passive shield is preferable. Since self-suppression is never 100% efficient, a net effect of the active shield contamination remains.

Individual cases depend on the suppression balance for detector impurities and for impurities from the active shield. Passive shielding is advantageous in that it is cheaper, has fewer construction constraints, and is more easily controlled for radioimpurities. Moreover, its long time stability is superior to that of electronic systems. Scintillation counting is especially sensitive to changes in temperature, both in PMT gain and in scintillation light output. Hence, temperature drifts can cause veto thresholds to vary. Long time stability is essential in cases in which the background is evaluated from extended measuring periods, e.g. in radiochemical solar neutrino experiments.

Background can be indirectly suppressed by modeling it in Monte Carlo simulations and subsequently subtracting it from the measured signal. However, computers modeling requires a thorough understanding of the experimental geometry and location of the characteristic backgrounds as well as of the complete implementation of all physical processes involved. Fiducial volume cuts are common in large-scale experiments as a means of excluding high-event regions of outside radiation, but they can also be used in smaller detectors providing spatial information. Segmented detector arrays also fall into that category. The tracking technique is a very powerful tool for background discrimination and will certainly play a more important role in future experiments.

5. BACKGROUND CHARACTERISTICS IN INDIVIDUAL EXPERIMENTS

5.1 *Solar Neutrino Experiments*

Radiochemical solar neutrino experiments involve two types of radioactivity background problems: (*a*) The neutrino target has to fulfill certain radiopurity requirements in order to keep side reactions low; and (*b*) an extremely low background in the counting device is needed in order to detect the few disintegrations per week of the neutrino capture product (the signal). Production from nonneutrino sources is largely dominated by the (p, n) reactions for which the protons may be secondaries induced by cosmic ray muons, fast neutrons, or residual radioactivities in the target.

5.1.1 CHLORINE EXPERIMENT The pioneering Homestake experiment of Davis and coworkers has enabled almost continuous observation of the solar neutrino flux above 0.841 MeV via the reaction $^{37}Cl(\nu_e, e^-)^{37}Ar$ since 1967 (123). Side reactions in the 380 m^3 perchlorethylene (C_2Cl_4) resulting from cosmic muons, from fast neutrons, and from α activity in the liquid and in the tank surface have been studied (123, 124). The reactions preceding $^{37}Cl(p, n)^{37}Ar$ can be the muon photonuclear reactions $(\mu^{\pm}, p)$ and $(\mu^{\pm}, n)$ followed by $^{35}Cl(n, p)$

(the latter applies to other neutron sources as well), and (α, p) for uranium and thorium contamination. Trace amounts of sulfur may contribute via the reaction $^{34}S\ (\alpha, n)^{37}Ar$.

The muonic contribution at a depth of 1480 m (4100 m.w.e. of standard rock) has been estimated from a series of measurements with a smaller amount of C_2Cl_4 at various shallow depths and with up to 4 tons of K in the form of KOH down to the full depth of the neutrino chamber. For K, the direct processes $^{39}K(\mu^{\pm}, \mu^{\pm}2n)^{37}K \rightarrow {}^{37}Ar$ and $^{39}K(\mu^{\pm}, \mu^{\pm}pn)^{37}Ar$ are used (125).

During construction of the Homestake detector, the interior walls of the steel tank and samples of the (evaporated) liquid were monitored for α activity to ensure that the levels were below the requirement, which corresponded to a production rate of less than 0.02 ^{37}Ar atoms/day. The total ^{37}Ar background production rate of 0.08 ± 0.03 atoms/day is primarily the result of muons. When this rate is subtracted from the total signal obtained in 94 individual extractions, a rate of 0.429 ± 0.043 ^{37}Ar atoms/day remains, which is ascribed to solar neutrinos. This rate corresponds to 2.28 ± 0.23 solar neutrino units (SNU $= 10^{-36}$ captures per second per target atom) (123).

The strong deviation of the measured signal from the 7.5 SNU expected for the standard solar model (SSM) (2) constituted the first "solar neutrino puzzle." This puzzle has persisted for more than 20 years and is now joined by the second solar neutrino puzzle, a deficit in ^{7}Be neutrinos (8).

After an accumulation time of 35–100 days, approximately 95% of the few ^{37}Ar atoms are removed from the 610 tons of C_2Cl_4 by purging with 410 m^3 of He for about 20 h. The extraction yield is determined with a carrier of about 0.1 cm^3 Ar. The He passes through a charcoal trap at liquid N temperature to absorb the Ar and is then returned to the tank (cyclic desorption).

After the Ar is released from the charcoal, it is purified by gas chromatography to remove ^{85}Kr and ^{222}Rn. In a second step, reactive gases as well as ^{3}H are gettered with heated titanium. Finally, the Ar is pushed into a miniaturized proportional counter (0.3–0.5 cm^3) together with 2–5% CH_4, and the decay of ^{37}Ar back to ^{37}Cl by electron capture is observed ($T_{1/2} = 35$ days). An assembly of such a Davis-type proportional counter is shown in Figure 7 (126). The active volume is formed by the 25-mm-long (Ø 4 mm) Fe cathode enclosed in a fused silica (quartz) envelope. The counting gas is placed into the envelope by means of Hg, which fills the capillary tubes below. When it is assembled and a center wire 0.025 (or 0.013) mm in diameter is fixed, the end plug (Figure 7) is fused to the cylindrical envelope. Its thin quartz window allows calibration with an external ^{55}Fe source. Up to four of these counters can be placed into the well of a large NaI(Tl) detector as an anticoincidence guard counter. The NaI(Tl) is housed in a 20-cm-thick Hg shield (held in a double-wall iron cylinder) during counting.

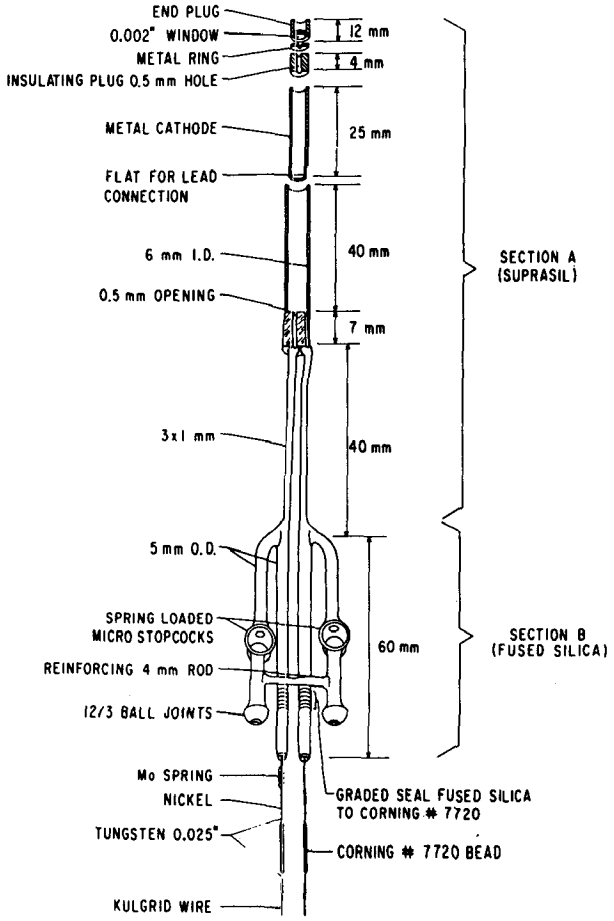

Figure 7 Assembly of a Davis-type proportional counter (126).

An important property of the Davis-type proportional counter, in addition to the low background resulting from the use of radiopure materials and from the small geometrical cross section against external radiation, is that it can be baked at 200–300°C. Baking removes volatile impurities that otherwise might alter the counting gas characteristics by outgassing during the long counting periods of 250–350 days. A hardware system recording the pulse energy, pulse rise time (amplitude of the differentiated pulse, or ADP), and the time difference between the energy and ADP peaking time helps reduce the background counting rate for the Auger electrons (2.82 keV total energy) to only 1–2 counts in 100 days

[one full width at half maximum (FWHM)]. The counting efficiency for ^{37}Ar under these conditions is 40–45%.

Two experiments based on the reaction $^{71}Ga(\nu_e, e^-)^{71}Ge$ with a threshold of 233 keV, which is well below the maximum energy of pp neutrinos ($E_{max} = 420$ keV) from the main fusion reaction in the Sun, have been monitoring solar neutrinos since 1990. SAGE (7), a Russian-American collaboration in the Baksan Underground Laboratory (4700 m.w.e. for the Ga chamber) (127), has used 30–57 tons of Ga in the form of liquid metal. The international GALLEX collaboration (6) operates a detector with 30.3 tons of Ga as 8.13 M aqueous $GaCl_3$ solution (101 tons) in the Gran Sasso Underground Laboratory (3400 m.w.e.) (128). The extraction techniques for both experiments were first worked out at Brookhaven National Laboratory (BNL).

5.1.2 GALLEX As in the Cl experiment, in GALLEX the few atoms of ^{71}Ge are purged out from the solution. Here, however, this is accomplished with 2000–3000 m^3 nitrogen in the batch desorption technique (129). In the end, GeH_4 is synthesized from tritium-free chemicals and used as a part of the counting gas. The average solar signal observed in the GALLEX experiment in 30 runs: 79 ± 10 (statistical) ± 6 (systematic) SNU (6). This value must be compared to the SSM values of 132 ± 7 SNU (130) or 124 ± 5 SNU (131), respectively. The contribution from side reactions corresponds to only about 6% of the observed signal.

The purity specifications for U and Th and for their progenies in the $GaCl_3$ solution were originally fixed at a 1% maximum contribution to the SSM production rate for each. ^{71}Ge production rates were measured with monoenergetic α particles from an accelerator incident in $GaCl_3$ solution (132). Tolerable activities of < 0.3Bq kg^{-1} for ^{238}U, < 8 mBq kg^{-1} for ^{232}Th, and < 19 mBq kg^{-1} for ^{226}Ra have been deduced. The reaction chain leading to ^{71}Ge is (α, p) on ^{69,71}Ga and ^{35,37}Cl followed by $^{71}Ga(p, n)^{71}Ge$. The production is strongly energy dependent; thus the 8.8 MeV of ^{212}Po (^{232}Th decay series) poses the most stringent limit. ^{226}Ra was treated separately since it could have been enriched during industrial Ga production.

Neutron activation analyses for U and Th, and Rn measurements for Ra, were performed on many individual samples and on total average samples, yielding concentrations well below the specifications (< 0.5 mBq ^{238}U kg^{-1}, < 0.2 mBq ^{232}Th kg^{-1}; ≤ 1.5 mBq ^{226}Ra kg^{-1}) (133). The contribution from internal U, Th, and ^{226}Ra is thus limited to less than the equivalent of 0.2 SNU. To test contamination with other α emitters and transuranic nuclides, highly sensitive Ge-γ spectrometry and α spectrometry were applied to aliquots of the target solution. In another method, an extraction measurement of fission Xe (^{133}Xe) from the full $GaCl_3$ solution was performed. Fast neutrons are about

one order of magnitude more efficient than α particles in ^{71}Ge production. These measurements enable spontaneous fission of transuranic nuclides to be excluded, with very good sensitivity, as an internal neutron source.

The environmental fast neutron (> 2.5 MeV) flux on the GALLEX side was measured with large BF_3 counters and determined to be $(0.23 \pm 0.07) \cdot 10^{-6}$ $cm^{-2}s^{-1}$ (87). In an independent measurement inside the empty tank, a similar flux was found to include neutrons from the tank wall as well. This measurement was done with a small radiochemical detector of 470 l $Ca(NO_3)_2$ solution (134). ^{37}Ar produced in the $^{40}Ca(n, \alpha)$ reaction has a much higher excitation function than that of ^{71}Ge in $GaCl_3$ solution, thus enabling the ^{71}Ge production rate to be scaled by the known production rate ratio. From these measurements we can conclude that the fast neutron contribution is equivalent to 0.15 ± 0.10 SNU (133, 134).

For penetrating muons, the relevant ^{71}Ge production rate in the $GaCl_3$ solution has been determined at the CERN muon beam (134). Together with the measured muon flux of 27 ± 3 $m^{-2}day^{-1}$ (135), this rate is estimated to be 3.7 ± 1.1 SNU in the target geometry (133, 134).

Many years of development and continuous refinement have led to a new counter design with a standardized quartz tube ($Ø_i = 6.4$ mm, 32.5 mm long) machined as the Fe or Si cathode to high precision. This new counter is based on the Davis-type proportional counter (Figure 7) and yielded a dead volume (not used for counting) of only 7%. Details of the counter development and its characteristics are given elsewhere (136).

The gas mixture (70% old Xe + 30% GeH_4 at 1.05 atm) was found to be the best compromise between counting characteristics such as efficiency, energy resolution, pulse form discrimination, background, and calibration performance.

After the counter is filled, it is embedded between two halves of low-activity lead (< 0.3 Bq ^{210}Pb kg^{-1}) that are part of the counter box (which holds the preamplifier, etc). The counter box is transferred through an air lock into the shield tank (Fe + Pb), which consists of a massive cylinder and two massive sliding front doors. Here it is placed either in 1 of the 8 positions inside a large well-type NaI(Tl) pair detector (active side) or in 1 of 29 wells of a highly radiopure Cu block (passive side). During the entire operation and the subsequent counting period, a Rn-free N atmosphere is maintained inside the shielding tank with the aid of a Rn monitor and suppression system (50, 137). All shield materials have been carefully screened for radioimpurities, primarily with Ge spectrometry (79). More details about the GALLEX spectrometer are given in Reference 137.

^{71}Ge decays via electron capture ($T_{1/2} = 11.43$ days), which results in peaks at 1.17 keV (L peak) and 10.37 keV (K peak). Each pulse is recorded in its

Table 3 Background sources of the GALLEX proportional counters and their induced count rates

Source	Activity or flux at the position of the proportional counter	Count rate > 0.5 keV (cpd)
External sources		
Muons	3×10^{-8} cm^{-2} s^{-1}	0.005
Neutrons	$< 10^{-6}$ cm^{-2} s^{-1}	< 0.001
Gamma rays	$< 10^{-6}$ cm^{-2} s^{-1}	< 0.02
Rn + progenies	< 0.5 Bq m^{-3}	< 0.006
K, Th, U in copper of the shielding material	< 2, 1, 1 mBq/kg	< 0.02
Internal sources		
K in quartz	0.04 mBq/kg	0.0001
Th in quartz	< 0.01 mBq/kg	< 0.0002
U in quartz	< 1.2 mBq/kg	< 0.03
^{60}Co in iron cathode	< 7 mBq/kg	< 0.02
K in iron cathode	0.06 mBq/kg	0.001
^{226}Ra in iron cathode	< 3 mBq/kg	< 0.2
Th in iron cathode	< 0.3 mBq/kg	< 0.017
U in iron cathode	< 0.4 mBq/kg	< 0.3
Tritium in counting gas	6 TU	0.023
^{85}Kr in counting gas	0.12 B1 m^{-3}	< 0.01
Sum		< 0.39

full shape with transient digitizers of different time scales. Every six to eight weeks, each counter is calibrated with fluorescent X rays induced in the Xe of the counting gas by an external ^{153}Gd-Ce target X-ray source. In this way, the entire counter volume is uniformly calibrated. All counting parameters controlled in this way have proved very stable (< 1%) over the full counting time (≥ 6 months).

Table 3 summarizes the most relevant background sources for the GALLEX proportional counter with an Fe cathode in the passive Cu shield (see 136 and 137 for details). The measured integral count rates are slightly higher, on average about 0.6 counts per day (cpd). These higher rates can be explained by the small radioimpurities introduced during the assembly and mainly during glass blowing, despite the fact that both are performed under clean-room conditions. After energy and rise-time cuts, the background count rate (passive side) is 0.04 cpd in the L peak (about 2 FWHM, 0.7–1.7 keV) and 0.02 cpd in the K peak (8.0–12.8 keV). The corresponding efficiencies for ^{71}Ge are about 31% and 35%, respectively.

The recognition efficiency for gas-internal ^{222}Rn decays is very high (91 ± 5%) from overflow events (α and high energy β) and from the time pattern of the decay sequence. Single ^{222}Rn decays can thus be detected.

In the positions of the NaI(Tl) pair detector, γ-active nuclides such as ^{68}Ge (^{68}Ga) and ^{69}Ge can be identified by various β-γ coincidence modes. However, this is done at the expense of a slightly higher background in the ^{71}Ge decay windows (primordial contamination in the PMTs).

5.1.3 SAGE The chemical extraction process from metallic Ga is based on the formation of an emulsion when a weak acidic solution, together with an oxidizing agent, is mixed into melted metallic Ga upon stirring (7). This mixing is performed in eight Teflon-lined chemical reactors holding together 57 tons of Ga. After several transfer steps, the extracted ^{71}Ge is placed in proportional counters (0.75 cm^3 active volume) as GeH_4. The overall extraction yield is typically 80% compared with about 99% in GALLEX.

The relevant muon and fast neutron fluxes are $2.23 \cdot 10^{-9}$ cm^{-2}s^{-1} and $5.3 \cdot 10^{-8}$ cm^{-2}s^{-1}, resulting in 0.4 SNU and < 0.06 SNU, respectively. As the laboratory is lined with low-background cement, the neutron flux from natural fission and (α, n) is reduced. The α activities (< 4 mBq ^{238}U kg^{-1}, < 1.7 mBq ^{232}Th kg^{-1}, and < 3 mBq ^{226}Ra kg^{-1}) are less effective in pure metal because of the absence of light target nuclides for (α, p) reactions, which feed the ^{71}Ga$(p, n)^{71}$Ge reaction. Furthermore, the favorable difference in redox potential results in a self-cleaning of the target so that in each run, uranium, radium, and thorium are extracted together with the dissolved Ga (0.1% of the total Ga). The disadvantage of this method is that substantial amounts of chemicals have to be added to the target in each run. Thus chemicals must be checked for radiopurity. The total side reaction rate in SAGE is ≤ 1.3 SNU (7).

Various types of proportional counters have been used at the beginning of the experiment. However, these counters could only measure the K peak at a background rate of 0.06–0.1 cpd (5). Starting with SAGE II, counters constructed of Suprasil quartz and zone-refined Fe cathodes came into use, together with a $9 \times 9''$ NaI(Tl) well-type crystal in a high-purity Cu/Pb shield. With the upgrade of the counting system, counter background rates were reached (138) that were similar to, e.g., GALLEX.

5.1.4 KAMIOKANDE The imaging water Čerenkov detector was originally designed to search for proton decay but was later upgraded to detect ^{8}B solar neutrinos by neutrino electron scattering (4, 139). The Čerenkov cone provides information on directionality, energy, and neutrino arrival time. Located at the Kamioka mine in the Japanese Alps, this detector is shielded by 2700 m.w.e. The Kamiokande detector consists of a cylindrical steel tank, with the main detector (2142 tons of water) viewed with 948 PMTs 50 cm in diameter, and a veto counter with 0.7–1.7 m (1800 tons) water viewed with 123 PMTs.

In order for ^{8}B neutrinos to be observed, the trigger rate of the PMTs had to be reduced by several orders of magnitude. This was achieved by identifying radioimpurities (U, Ra, Th, and Rn) from the water either through energetic electrons resulting from β decay or with Compton-scattered γ rays and by sealing the detector against Rn influx (190–1900 Bq m^{-3} in mine air). In addition, many other signal cuts were applied. The water purification system with ion-exchange colums, a mixed-bed-type deionization, and a degassification (vacuum extraction of Rn) system reduced the concentration of ^{226}Ra to about 4 mBq m^{-3}, that of U and Th to below 2 mBq m^{-3}, and that of ^{222}Rn to about 30 Bq m^{-3} (140). Uranium required special attention since it releases about 7.2 MeV of energy in the form of prompt γ rays upon spontaneous fission. The anticounter reduced the rate of γ rays in the detector from the surrounding rock by a factor of about 100. Remaining γ rays and those that have been converted to charged particles near the walls of the detector are removed by a fiducial volume cut (680 tons). Further cuts remove spallation products from O, such as the short-lived ^{16}N, by through-going muons, as well as products of stopped negative muons, by space and time correlations.

With these reductions of background and the ability to point back to the direction of the neutrinos, Kamiokande provided the first pointed observation (neutrino heliograph) of neutrinos coming from the Sun. The signal corresponds to 0.50 ± 0.04 stat. ± 0.06 syst. of the SSM flux (141).

5.1.5 FUTURE SOLAR NEUTRINO EXPERIMENTS Superkamiokande is an improved and enlarged (22,000 tons fiducial volume) version of the Kamiokande detector that further reduces uranium, radium, and thorium impurities and substantially reduces radon concentration (141).

The Sudbury Neutrino Observatory (SNO) is based on a 1000-ton heavy-water (D_2O) Čerenkov detector located in the Creighton mine in Sudbury, Canada, at a depth of 5900 m.w.e. (22). The D_2O target can be sensitive to all types of neutrinos via the neutral current (NC) reaction $\nu_x + d \rightarrow \nu_x + p + n$. The neutron will be detected either by the capture reaction $^{35}\mathrm{Cl}(n, \gamma)$, which produces 8-MeV γ rays, or with ^{3}He proportional counters. In the first scenario, NaCl will be admixed to the D_2O. SNO will also observe the charged-current (CC) reaction $\nu_e + d \rightarrow p + p + e^-$, which is sensitive only to electron neutrinos, and, like Kamiokande, the neutrino elastic scattering reaction $\nu_x + e^- \rightarrow \nu_x + e^-$, which has a higher sensitivity (ca 7×) for electron neutrinos compared with that for μ and τ neutrinos. The heavy water will be contained in a spherical acrylic vessel (Ø 12 m, 5-cm wall thickness), which is viewed with an array of 9600 PMTs 50 cm in diameter immersed in a water shield of 7300 tons. The cavity enclosing the light water shield is lined with low-background concrete (0.1 Bq ^{238}U kg^{-1}; 45 mBq ^{232}Th kg^{-1}) (142) to shield

neutrons and γ rays from the norite rock. Rn emanation into the water from the concrete is suppressed by a waterproof plastic liner with low Rn permeability. The NC reaction, characterized by the release of a detectable neutron competes with background from neutrons, either entering the D_2O vessel either from the outside, or from (α, n) reactions of U and Th impurities in the tank or from deuteron photodisintegration induced by γ ray with energy larger than 2.223 MeV. This background imposes stringent purity specifications for D_2O, H_2O, and the acrylic (10^{-14} to 10^{-12}g U/Th g^{-1}) and requires ultimate cleanliness during the construction phase in order to avoid contamination with dust etc.

A system has been developed to extract Ra and Th by filtering the water with Mn-coated beads. This technique is widely used to study Ra and Th in environmental water.

Measurements have been made on all major components of the detector. The acrylic has been assayed for U and Th by mass spectrometry and α counting after vaporization of 1–10 kg and by neutron activation (22, 143). Many materials have also been studied for their ^{222}Rn emanation (101). The envelope of the PMTs is made from a special melt of low-activity glass (1 Bq ^{40}K kg^{-1}, 0.2 Bq ^{238}U kg^{-1}, and 0.07 Bq ^{232}Th kg^{-1}) manufactured by Schott.

Borexino, another future solar neutrino real-time detector, is based on liquid scintillation and specially tuned to the monoenergetic 860-keV ^{7}Be neutrinos. In order to observe elastic electron scattering of neutrinos at this low-energy domain of natural activity, extreme radiopurity levels in the liquid organic scintillator must be met ($< 10^{-15}$ g U/Th g^{-1}; $< 10^{-14}$ g K g^{-1}). A vessel made from transparent nylon contains 300 tons of scintillator (100 tons fiducial volume). It is viewed with 1700 PMTs (Ø 200 cm) mounted to a steel sphere filled with mineral oil as a buffer. This steel sphere is again contained in a cylindrical steel tank (Ø 17 m, 17 m high) filled with shielding water (144). The conceptual design features shells of increasing purity moving from the water to the scintillator. A smaller-scale device with 4 tons of scintillator and without the mineral oil buffer, called the Counting Test Facility (CTF), has been constructed in the Gran Sasso Underground Laboratory to demonstrate that the required purity can be reached. Its flexible nylon vessel is viewed with 100 PMTs supported by an open structure in the shielding water. The outer steel tank has a diameter of 11 m and is 10 m high. It is hoped that the CTF will also provide information on the ^{14}C concentration in the scintillator (pseudocumene + PPO), which should be in the range of $^{14}C/^{12}C = 10^{-18}$ or lower in order for Borexino to have a reasonably low trigger threshold. The CTF will also test the recognition power for the natural decay chains and other contaminants by delayed coincidences for the application of background cuts. The spatial resolution will be studied as well. Earlier laboratory-scale investigations with

another scintillator base (trimethylborate, TMB) proved that the required purity levels for U, Th, and K can be reached. These investigations have also led to the development of an efficient repurification technique (Methex) (145).

In a large-scale experiment, the surface-to-volume ratio is more favorable for high purity levels; thus the realization of Borexino seems feasible. The radiopurity specifications of the shielding water (10^{-13}g U/Th g^{-1}, 10^{-10}g K g^{-1}) have already been met by a water system consisting of reverse osmosis and continuous deionization. The analytical method is ICPMS with a preconcentration step for the scintillator measurement (145). The specification for the ^{222}Rn concentration in the water and in the scintillator (1 mBq m^{-3}, < 10 μBq m^{-3}) hopefully will be achieved via flushing these liquids with N_2. To monitor such low concentrations independent of direct measurement with the CTF, Rn is extracted with N_2, collected on a charcoal (1 mBq ^{226}Ra kg^{-1}) trap, and subsequently counted in a Davis-type proportional counter.

These and other future solar neutrino experiments are described in References 5 and 146.

5.2 *$\beta\beta$ Decay and Dark Matter Experiments*

5.2.1 *$\beta\beta$ DECAY* Compared with solar neutrino experiments, $\beta\beta$ experiments are still small scale. Both the neutrinoless (0ν) $\beta\beta$ decay and dark matter experiments are exclusion experiments since up to now no positive evidence has been observed in either class of experiment. The background for a certain energy region from which the exclusions are derived is given as "counts $(\text{keV} \cdot \text{kg} \cdot \text{year})^{-1}$" or in equivalent units. Since the sources of background for both experiments are those discussed in Sections 2 and 3, a direct comparison is possible using this figure. Neutrinoless $\beta\beta$ decay, if it exists, can produce a sharp line that is more easily recognized than the continuous distribution from nuclear recoil of WIMPs.

Searches for the 0ν spike involve a search for excess counts above a statistically fluctuating background so that the lower limit for the half-life derived from this background is

$$T_{1/2} > ci(Mt)^{1/2}(br)^{-1/2}. \qquad 1.$$

The effective (Majorana) neutrino mass $\langle m \rangle$ is related to this $T_{1/2}$ by

$$\langle m \rangle = dT_{1/2}^{-1/2}, \qquad 2.$$

where c and d are constants not discussed here, i is the isotopic abundance, M is the active mass, t is the measuring time, b is the background, and r is the energy resolution. These relations show the importance of isotopic enrichment compared with the other parameters.

Here we outline only a few examples of experiments working with enriched isotopes and searching for the $0^+ \rightarrow 0^+$ transition in $0\nu\ \beta\beta$ decay. These experiments are the most sensitive because they use isotopically enriched material and large active masses and because they yield the lowest background rates.

5.2.2 HEIDELBERG-MOSCOW ^{76}Ge $\beta\beta$ COLLABORATION Five Ge crystals (0.92–2.8 kg) isotopically enriched to a ^{76}Ge abundance of about 86–88% are in operation at the Gran Sasso Underground Laboratory (14, 44, 69). The use of enriched material in this source-equals-detector calorimetric approach also strongly depletes ^{70}Ge (20.5% $\rightarrow <$ 0.1%). Consequently, the persistent background in normal isotopic experiments from cosmogenic ^{68}Ge ($T_{1/2} = 271$ days) produced via ^{70}Ge$(n, 3n)^{68}$Ge is strongly reduced. The energy released in the β^+ decay of the daughter of ^{68}Ge, ^{68}Ga may extend beyond the ^{76}Ge Q-value of 2.0386 MeV. All crystals are mounted in individual cryostats made from one batch of high-purity Cu that was stored underground shortly after electrolysis and final melting. Its radiopurity was tested before the order was placed. All other materials used for the construction of the cryostat and the shield were screened and selected, primarily with Ge spectrometry (44, 79). This also holds true for all other experiments described below. Exposure to cosmic rays was minimized for the Ge crystals and for other materials whenever feasible. Electrobeam welding was the only joint technique employed. Prior to the assembly of the cryostat in a clean room, all parts were either electropolished or acid cleaned. For vacuum sealing, a low-activity lead wire was used. The electronic components (cooled FET, etc.) are placed far away from the crystal and outside the lead shield. Four of the crystals are mounted in one common lead shield made of 20 cm LC2 lead and 20 cm Boliden lead. The fifth crystal is housed in a Pb/Cu shield. Rn influx from the laboratory air is prevented by a tight steel hood around the lead shields that is sealed to a floor plate. N_2 gas is continually flushed with slight overpressure into the center of the shield.

At the beginning of the measurement, cosmogenic radioisotopes such as ^{58}Co, ^{57}Co, ^{54}Mn, and ^{65}Zn dominated the spectrum, although their activity was only a few percent of the saturation activity in Ge or in Cu at sea level (Table 1). As a result, the background count rate gradually declined from the decay of these isotopes. Later, predominantly the primordials (K, U, and Th) remained, as can be seen in Figure 8. This figure shows that the background can be reduced dramatically by shielding, underground operation, and great care in radiopurity. The upper spectrum was measured unshielded at the low-level laboratory of the Max-Planck-Institut for Nuclear Physics in Heidelberg (60), and the lower one was measured in the pure lead shield at the Gran Sasso Laboratory. Despite the reduction by five orders of magnitude, the spectra resemble each other and feature the same lines, except that the ^{137}Cs line (661.7 keV) is more pronounced

in the lower spectrum, and the ^{60}Co lines (1173.2 + 1332.5 keV) are present only in this spectrum. Even at this extreme low-radioactivity level, the primordials are still the main limiting factor for further background reduction. The statistics in the lines of the U and Th decay series are too low to locate this contamination by Monte Carlo simulation in some of the materials near the crystal. Thus, surface contamination cannot be ruled out. Even if the activity is completely placed into the Cu, a U and Th contamination well below 100 μBq kg^{-1} would result (148). The long-time average background between 2000 and 2080 keV is at this time (January 1995) 0.2 counts (keV · kg · year)$^{-1}$. The recent completion of a neutron shield (10 cm borated polyethylene on all sides) seems to have reduced this background even further. It is hoped that pulse-shape analysis will result in additional improvement (149). Because contribution of a shorter-lived cosmogenic isotope cannot be fully excluded, the first 200 days of counting of each detector are not included in the data analysis.

In the International Germanium Experiment (IGEX), several smaller enriched Ge crystals have been tested at different underground locations (150). Phase II detectors (> 2 kg) are undergoing tests in cryostats made from electro-

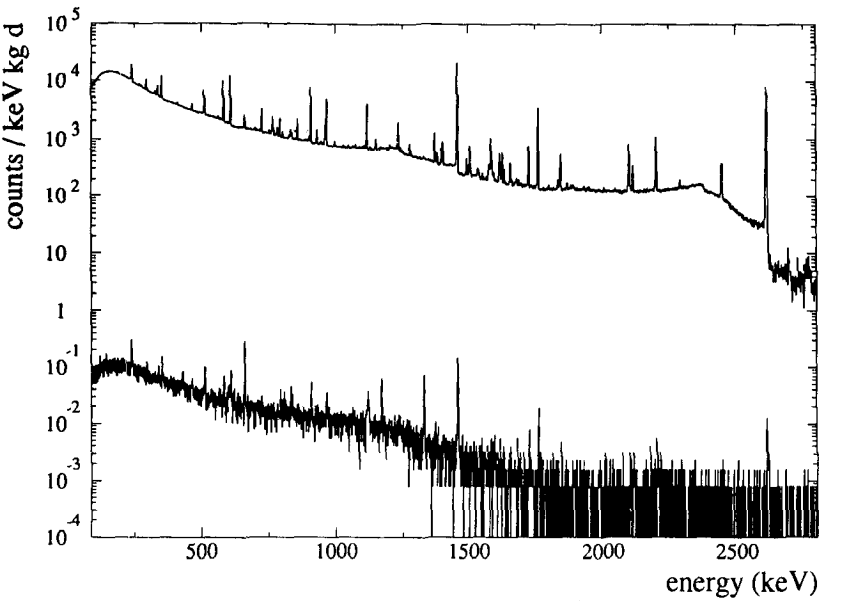

Figure 8 Background spectra of an enriched Ge detector of the Heidelberg-Moscow collaboration (2.3 kg active volume) unshielded at 15 m.w.e. (*top*) and shielded with 40 cm lead at 3400 m.w.e. (*bottom*).

formed Cu with improved radiopurity. The background seems to be comparable to that in the Heidelberg-Moscow Experiment. At this time it has still low statistics (RL Brodzinski, private communication).

Another source-equals-detector approach but with additional tracking capabilities is the high-pressure ^{136}Xe time projection chamber of the California Institute of Technology (Caltech)–Neuchâtel–Paul Scherrer Institute (PSI) collaboration (151). The experiment is performed in the Gotthard Underground Laboratory (about 3000 m.w.e.) with 5 atm xenon enriched to 62.5% in the $\beta\beta$-active ^{136}Xe. A $\beta\beta$ decay event produces a continuous trajectory with the characteristic end features (high-charge depositions) of electrons at both ends. This specific signature is a powerful means of background suppression from α particles, muons, and single electrons. However, it is not possible in 5 atm of such heavy gas to measure the momentum and charge from magnetic curvature as it was applied in the pioneering Time Projection Chamber experiment of Moe and collaborators (152). These authors observed for the first time the 2ν $\beta\beta$ decay by direct counting.

The main chamber is a cylindrical OHFC Cu vessel with 5 cm wall thickness. It is shielded with 20–30 cm of Pb. A background source unique to this experiment is that of thermal neutrons forming the high-energy β emitter ^{137}Xe via $^{136}\mathrm{Xe}(n, \gamma)^{137}\mathrm{Xe}$. The thermal neutron flux is attenuated by the Pb/Cu shield by a factor of 10^3. The muonic background component is controlled by a veto ring in the TPC. Although the energy resolution at the 2481-keV Q-value is a factor of 45 worse than it is in Ge, this disadvantage is mitigated by the lower background [about 0.01 counts $(\mathrm{keV} \cdot \mathrm{kg} \cdot \mathrm{year})^{-1}$] due to the tracking information. In a recent upgrade, the background was improved about fivefold, primarily by crimping the wires instead of using solder (153).

In the NEMO (Neutrino Experiment in Molybdenum) project, source and detector are separated. A calorimeter/tracking version is being realized in three steps at the Fréjus Underground Facility (Laboratoire Souterrain de Modane, LSM) (4800 m.w.e.) (154). In the NEMO I and II detectors, tracking with multiwire Geiger drift tubes and plastic scintillators (which provides energy and time-of-flight information) has been studied, as have various sources of background. The design of NEMO III consists of both an inner and outer cylinder of plastic scintillator arrays with the source foil (3.1 m in diameter and 2 m high) in between. The tracking volume on both sides of the cylindrical source foil is formed by the space between the foil and the plastic scintillator arrays. The first priority is to measure 10 kg of 98% ^{100}Mo (Q-value = 3.03 MeV), but other isotopes, in particular ^{96}Zr, ^{116}Cd, and ^{150}Nd, are being considered as well (154).

5.2.3 DARK MATTER SEARCH Dark matter search experiments are rapidly evolving, but up to now the most sensitive measurements have come from detectors

originally developed for $\beta\beta$ decay experiments (155). The event rates range from 0.1 to 1 count $(\text{keV} \cdot \text{kg} \cdot \text{day})^{-1}$ in the energy region of 10 keV. Only for axial-coupling interaction (or spin-spin interaction) scintillation detectors have reached higher sensitivity than conventional Ge detectors (156). Here, progress was made through the development of NaI(Tl) crystals of higher radiopurity (< 2 mBq ^{40}K kg^{-1}; ~ 20 μBq kg^{-1} ^{238}U/^{232}Th) and low-background photomultipliers (156). Liquid gas (Xe) counting has also been undertaken by various groups (157).

In the near future the first cryogenic dark matter searches will come on-line together with new background discrimination techniques (also for conventional detectors), as indicated in Section 4.3. We refer to the recent reviews of the status in dark matter search (158, 159). In cryogenic experiments, the difficulties of low radioactivity are joined by the difficulties of the sophisticated technology of low-temperature physics.

The first experiments along these lines will presumably be performed with the detector at the Center for Particle Astrophysics at Berkeley, which uses the calorimetry + ionization method on ^{73}Ge (158), and with two purely calorimetric detectors (Al_2O_3-sapphire), one developed by the French collaboration (160) and the other by the Munich group (161). Only the latter two will be operated deep underground.

6. FUTURE PROSPECTS AND BENEFIT TO OTHER FIELDS

In the past two decades, remarkable progress has been made in low-radioactivity background techniques, triggered mainly by rare-event experiments. This development was paralleled by advances in technologies designed to meet the demand of the electronic industry for radiopure materials. Larger-scale experiments will likely merge divergent interests of multiple groups and thus enable further progress. Radioassay techniques have considerably advanced, especially in mass spectroscopy, making bulk analysis of all types of materials in the parts per trillion (ppt) (μBq kg^{-1}) range feasible. Final limitations will not be determined by bulk radiopurities but rather by the problem of surface contamination. Future cryogenic detectors will have higher surface-to-volume ratios from thermal radiation shields. This ratio will be even more pronounced in detectors based on micron size superconducting granules (16).

The probable avenues of future rare-event research are discussed below. The most advanced semiconductor (Ge) solid-state ionization systems operate at the μBq kg^{-1} level. Work in this field indicated that a temporary stop in further background reduction arises from surface contamination, although this has not

yet been proved. To overcome this obstacle, more sophisticated surface cleaning techniques as well as higher sensitivity in monitoring surface contaminations are needed. Help may come in the form of extreme clean-room environments such as those applied in industrial wafer production and in cleaning technologies developed in that field (162). Low-radioactivity background experiments of the next generation will require clean-room installations in underground laboratories so as to also minimize cosmogenic activation during assembly.

If Borexino succeeds in reaching 10^{-16}g g^{-1} U/Th (nBq kg^{-1}) in the scintillator, new ground will be broken. In addition to even more radiopure PMTs or photodiodes of higher sensitivity, smaller-scale scintillation experiments would become attractive in rare-event research. The handicap of low-energy resolution is partly compensated by the high counting efficiency if the nuclide of interest is admixed to the scintillator. To develop PMTs with higher radiopurities, experimentalists should join forces to raise commercial interest. The contamination level of the lowest background glass is still in the range of a few 100 mBq kg^{-1} for ^{40}K/^{238}U/^{232}Th. The inner components (especially the ceramic insulators) have even higher specific activities. The use of light guides made from radiopure quartz, for example, comes at the expense of losses in energy resolution. Other joint efforts could concentrate on the fabrication of low-activity solder with a K-free flux core or the development of common stock lists of radiopure materials for interlaboratory exchange.

Liquid gas counting will also be more widely applied in future experiments. Here, the obstacles of Rn contaminations and of other rare gases must be mastered before lower background can be achieved. ^{42}Ar ($T_{1/2} = 32.9$ years) is the only longer-lived relevant nuclide with a decay energy exceeding 1 MeV (from its daughter ^{42}K).

The progress made in low-activity Ge spectrometry would not have been possible without the close cooperation of the manufacturers. This cooperation has also enabled industry to offer low-background versions of their detectors for broader application. In addition, more reasonable detector shields have become available. The life sciences in particular have profited from this development. In this field, however, interest in achieving still lower background levels is unlikely since turnover times are much shorter, making an improvement in efficiency more beneficial.

The speed of further technical progress will depend on additional developments in rare-event research. Therefore, the future directions of this field are addressed below.

6.1 *Future Rare-Event Experiments*

It is hoped that the upcoming direct counting solar neutrino experiments (SNO, Superkamiokande, and Borexino) will shed more light on the solar neutrino

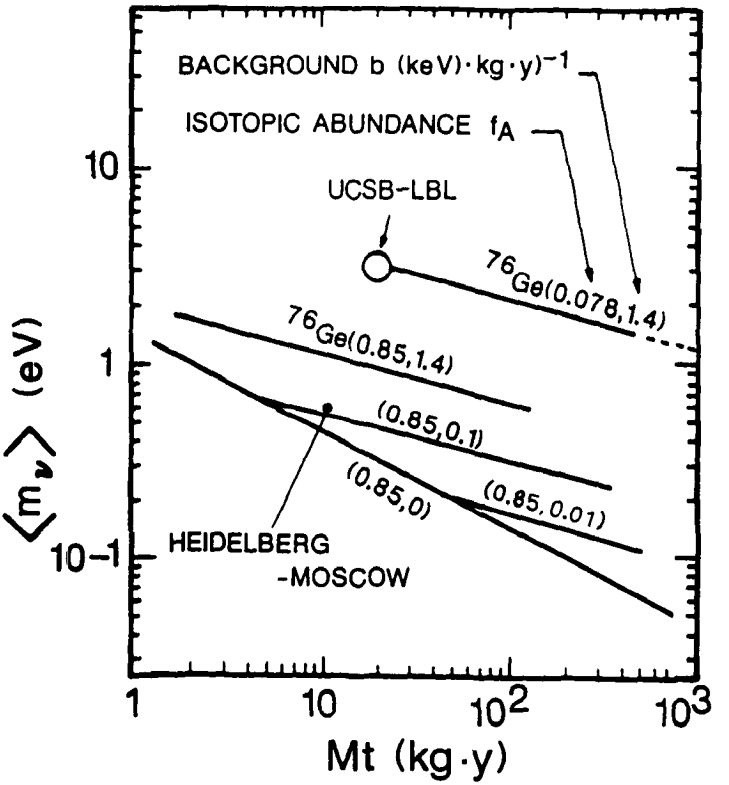

Figure 9 Minimal effective neutrino mass vs the product (detector mass × measuring time) for normal isotopic and enriched ^{76}Ge at various background rates.

problem (8), but the interest in measuring the entire solar neutrino spectrum with good resolution will certainly result in additional solar neutrino experiments (146). The liquid Ar tracking detector ICARUS will be sensitive only to ^{8}B neutrinos but will have improved energy resolution compared with SNO and Superkamiokande. In the more distant future, cryogenic detectors with low thresholds, very good energy resolution, and good tracking capabilities hopefully will begin operation.

In $\beta\beta$ decay, the situation is well illustrated by the diagram of Moe (147) which is reproduced in Figure 9. It shows the minimum detectable neutrino mass as a function of the product: detector mass × measuring time for normal isotopic and enriched Ge detectors of various levels of background (according to Equations 1 and 2 of Section 5.2). Only with the unrealistic assumption of zero background could the mass sensitivity increase with the square root of this product.

The present (January 1995) status of the Heidelberg-Moscow experiment is indicated in Figure 9. A further reduction of the background by one order of magnitude might not be completely unrealistic, but this will only improve the mass limit by less than a factor of two because of the dependence on the fourth root. One option for background reduction is to immerse the almost bare crystals in liquid N, which would serve as a shield. A few tenths of eV for $\langle m_\nu \rangle$ will be the limit for ^{76}Ge calorimeters. The design goal of NEMO III is about 0.1 eV. Major improvements beyond that point are only possible with large-scale experiments with drastically higher discrimination power. In the long term, these will again be cryogenic detectors with much better energy resolution and high-resolution tracking characteristics. In the shorter term, projects are envisioned that can not only detect the decay but also tag the decay product, e.g. ^{136}Ba, the daughter of ^{136}Xe (M Moe, private communication). The resonance ionization spectroscopy (RIS) technique may be one option that can be implemented in the $\beta\beta$ decay detection device.

In WIMP search with direct detection, cryogenic detectors are needed in order to probe masses below 10 GeV (161). The options for background discrimination in the large variety of cryogenic detectors make this technology the best prospect for the future in this class of experiments as well (15, 158, 159). Cryogenic detectors with tracking capabilities could make use of modulations from the Earth's orbital motion through the galactic halo (of WIMPs) (16, 158).

Expected sensitivity levels for future dark matter experiments range from 10^{-4} to 10^{-1} event kg^{-1} day^{-1} (158, 159). This is several orders of magnitude below present background levels. Frontiers in modern physics are moving toward rarer and rarer events that are currently hidden behind the curtain of noise and background (better characterized by the French expression "bruit de fond"). We had better make careful use of superlatives (ultralow...) so as not to run out of suitable expressions for future background levels. Let us proceed, therefore, as unexpected physics may appear between 2ν $\beta\beta$ decay and dark matter recoil or before the background is immersed in neutrino interactions.

ACKNOWLEDGMENTS

This article is dedicated to my wife Lilo. I thank her for the support and patience during its preparation. I acknowledge the valuable discussions with my colleagues at GALLEX, at the Heidelberg-Moscow Collaboration, and at Borexino. Special thanks go to Wolfgang Hampel in that respect. I am indebted to Till Kirsten for critical reading and for stylistic improvements. The contribution on chemical information by Ernst Pernicka is greatly appreciated. Colleagues who provided direct information on their experiments and preprints are thanked. I would also like to acknowledge the help of Brigitte Schulz in the preparation of the text.

Literature Cited

1. Sutton Ch. *Spaceship Neutrino.* Cambridge: Cambridge Univ. Press (1992)
2. Bahcall JN. *Neutrino Astrophysics.* Cambridge: Cambridge Univ. Press (1989)
3. Davis R Jr, Mann AK, Wolfenstein L. *Annu. Rev. Nucl. Part. Sci.* 39:467 (1989)
4. Hirata KS, et al. *Phys. Rev. D* 44:2241 (1991)
5. Bowles TJ, Gavrin VN. *Annu. Rev. Nucl. Part. Sci.* 43:117 (1993); Cremonesi O. Rivista del *Nuovo Cimento* 16:1 (1993)
6. GALLEX collaboration, Anselmann P, et al. *Phys. Lett. B* 327:377 (1994)
7. Abdurashitov JN, et al. *Phys. Lett. B* 328:234 (1994)
8. Kirsten TA. *Proc. Int. Workshop Solar-Neutrino Problem: Astrophysics or Oscillations*, ed. V Berezinsky, E Fiorini (1994); Hata N, Bludman S, Langacker PG. *Phys. Rev. D* 49:3622 (1994); Bahcall JN. *Phys. Lett. B* 338:267 (1994); Berezinsky V, Fiorentini G, Lissia M. *Phys. Lett. B* 34:38 (1994)
9. GALLEX collaboration, Anselmann P, et al. *Phys. Lett. B* 342:440 (1995)
10. Mikheyev SP, Smirnov AY. *Nuovo Cimento* 9C:17 (1986); Wolfenstein L. *Phys. Rev. D* 17:2369 (1978)
11. Moe M, Vogel P. *Annu. Rev. Nucl. Part. Sci.* 44:247 (1994)
12. Fiorini E, et al. *Phys. Lett. B* 25:602 (1967)
13. Vasenko AA, et al. *Mod. Phys. Lett. A* 5:1299 (1990); Balysh A, et al. *Phys. Lett. B* 283:32 (1992); Klapdor-Kleingrothaus HV, *Prog. Part. Nucl. Phys.* 32:261 (1994)
14. Balysh A, et al. *Proc. 27th Int. Conf. on High Energy Physics*, Glasgow, 1994, ed. PJ Bussey, IG Knowles, p. 939 Bristol: IOP Publishing (1995)
15. Primack JR, Seckel D, Sadoulet B. *Annu. Rev. Nucl. Part. Sci.* 38:751 (1988)
16. Smith PF, Lewin JD. *Phys. Rev.* 187:203 (1990)
17. Heusser G. *Nucl. Instr. Methods Phys. Res. B* 17:418 (1986)
18. Heusser G. *Proc. Int. Summer School, Low-Level Measurements of Radioactivity in the Environment, 3rd, Huelva, 1993,* ed. M Garcia-Leon, R Garchia-Tenorio, p. 69. Singapore: World Scientific (1994)
19. Beck HL. *Proc. Natural Radiation Environment, 2nd, Houston, 1972,* ed. JAS Adams, WM Lowder, TF Gesell, p. 101. Oak Ridge: US At. Energy Comm. (1975); see also Ref. 48 and *The Natural Radiation Environment*, ed JAS Adams, WM Lowders. Chicago: Univ. Chicago Press (1964)
20. National Council on Radiation Protection and Measurement. *Rep. Nr. 94.* Bethesda, MD (1987)
21. Ivanovich M, Harmon RS, eds. *Uranium Series Disequilibrium: Applications to Earth, Marine and Environmental Sciences.* Oxford: Clarendon (1992)
22. Sudbury Neutrino Observatory proposal, Kingston (1987)
23. Lal D, Peters B. In *Encyclopedia of Physics,* ed. S Fluegge, K Sitte, 46(2):551. Berlin: Springer (1967)
24. Lal D. *Annu. Rev. Earth Planet. Sci.* 16:355 (1988)
25. Caldwell DO, et al. *Phys. Rev. Lett.* 65:1305 (1990); Plaga R. *Nucl. Instrum. Methods Phys. Res. A* 309:598 (1991)
26. Weiss W, Sartorius H, Stockburger H. *Proc. Consultants' Meeting on Isotopes of Noble Gases as Tracers in Environmental Studies, Vienna, 1989,* p. 29. Vienna IAEA (1992)
27. De Voe JR. *Radioactive Contamination of Materials used in Scientific Research, NAS-NCR-Pub-895. Nucl. Sci. Ser. Rep. Nr. 34* (1961)
28. Wogmann NA, Laul JC. *Proc. National Radiation Environment, Bombay,* ed. KG Vohra, et al, p. 384. New Delhi: Wiley (1981)
29. Jagam P, Simpson JJ. *Nucl. Instr. Methods Phys. Res. A* 324:389 (1993); Brodzinski RL, et al. *Nucl. Instr. Methods Phys. Res. A* 239:207 (1985); Avignone FT, et al. *Phys. Rev. C* 34:666 (1986); Reeves JH, et al. *IEEE Trans. Nucl. Sci.* 31:697 (1984)
30. Dunlop JA, et al. *JOM* 18 (June 1989)
31. de Vries HL, Bardensen GW. *Physica* 19:987 (1953)
32. Weller RI, Anderson EC, Barker JL Jr. *Nature* 206:1211 (1965)
33. Bartels OG. *Health Phys.* 28:189 (1975)
34. Weller RI. *Health Phys.* 41:15 (1981)
35. Kolb WA *Environ. Int.* 14:367 (1988)
36. Eisenbud M. *Environmental Radioactivity.* New York: Academic (1973)

37. Wojcik M. *Nucl. Instrum. Methods* 189:645 (1981)
38. Zastavny A, Bialon J, Sosinski T. *Appl. Radiat. Isot.* 40:19 (1989)
39. de Boeck R, Adams F, Hoste JJ. *Radioanal. Chem.* 1:397 (1968)
40. Brodzinski RL, et al. *Nucl. Instrum. Methods Phys. Res. A* 254:472 (1987)
41. Bunzl B, Kracke W. *Nucl. Instrum. Methods Phys. Res. A* 238:131 (1985)
42. Alessandrello A, et al. *Nucl. Instrum. Methods Phys. Res. B* 61:106 (1991)
43. Alessandrello A, et al. *Nucl. Instrum. Methods Phys. Res. B* 83:539 (1993)
44. Balysh A, et al. *Phys. Lett. B* 322:176 (1994)
45. Brodzinski RL, et al. *Nucl. Instrum. Methods Phys. Res. A* 239:207 (1985)
46. Reineking A, Postendörfer J. *Health Phys.* 58:715 (1990)
47. Heusser G. *Nucl. Instrum. Methods Phys. Res. B* 58:79 (1991)
48. Gogolak CV, Beck HL. *Proc. Natural Radiation Environment, 3rd, Houston, 1978,* ed. TF Gesell, WM Lowder. p. 259. Tech. Inf. Cent., US Dep. Energy (1980)
49. Postendörfer J, Butterweck G, Reineking A. *Health Phys.* 67:283 (1994)
50. Heusser G, Wojcik M. *Appl. Radiat. Isot.* 43:9 (1992)
51. Müller W. *Die Diffusions-, Löslichkeits- und Permeabilitätskoeffizienten von Radon 222 in handelsüblichen Kunststoffen.* Staatsexamensarbeit, Univ. Heidelberg (1978)
52. Wojcik M. *Nucl. Instrum. Methods Phys. Res.* B61:8 (1991)
53. Gerrard W. *Gas Solubilities, Widespread Applications.* The Polytechnic of North London, Oxford: Pergamon, p. 162 (1980)
54. Simpson JA. *Annu. Rev. Nucl. Part. Sci.* 33:323 (1983)
55. Allkofer OC, Grieder PKF. *Cosmic Rays on Earth, Physics Data Nr. 25-1* (1984)
56. Gaisser TK. *Cosmic Rays and Particle Physics.* Cambridge: Cambridge Univ. Press (1990)
57. Gorshkov GV, et al. *Natural Neutron Background of the Atmosphere and the Earth Crust* (in Russian). Moscow: Atomizdat (1966)
58. Grupen C. *Z. Fortschr. Phys.* 23:127 (1976); *Landolt-Börnstein. Numerical Data and Functional Relationships in Science and Technology, New Series,* Group 1: *Nuclear and Particle Physics, Vol. 11: Shielding against High Energy Radiation* (1990) ed. H Schopper. Berlin: Springer; Bilokon H, et al. *J. Geophys. Res.* 94:12, 145 (1989)
59. Cassiday GL, Keuffel JW, Thomson JA. *Phys. Rev. D* 7:2022 (1973)
60. Heusser G. 1992. *Proc. Europhys. Conf. on Nuclear Physics and Rare Nuclear Processes, 14th, Bratislava, 1990,* ed. P Povinec, p. 247. Singapore: World Scientific (1992)
61. Beck M, et al. *Phys. Rev. Lett.* 70:2853(1993)
62. Avignone FT III, et al. *Phys. Rev. C* 34:666 (1986)
63. Fisher P, et al. *Phys. Lett. B* 218:257 (1992)
64. Signer P, Nier AO. *J. Geophys. Res.* 65:2947 (1960); Reedy RC, Arnold JR, Lal D. *Annu. Rev. Nucl. Part. Sci.* 23:505 (1983); Vogt S, Herzog GF, Reedy RC. *Rev. Geophys.* 28:253 (1990); Michel R, et al. *J. Radioanal. Nucl. Chem.*169:13 (1993)
65. Faure G. *Principles of Isotope Geology.* New York. Wiley. 2nd ed. (1986); Cerling TE, Craig H. *Annu. Rev. Earth Planet. Sci.* 22:273 (1994)
66. Gehrels N. *Nucl. Instrum. Methods Phys. Res.* A239:324 (1985), A292:505 (1990), A313:513 (1992); Dean AJ, Lei F, Knight PJ. *Space Sci. Rev.* 57:109 (1991)
67. Silberberg R, Tsao CH. *Phys. Rep.* 191:353 (1990)
68. Brodzinski RL, et al. *Radioanal. Nucl. Chem.* 124:513 (1988); Avignone FT III, et al. *Nucl. Phys. B* 28A(Proc. Suppl.):280 (1992)
69. Balysh A. *Proc. Rencontre de Moriond. Progress in Atomic Physics, Neutrinos and Gravitation, 27th, Les Arces, 1992,* ed G Chardin, O Fackler, J Tran Thanh Van, p. 177. Gif-sur-Yvette: Frontières (1992)
70. Martoff CJ. *Science* 237:507 (1987); Martoff CJ, Lewin PD. *Comp. Phys. Comm.* 72:96 (1992)
71. Hampel W. *AIP Conf. Proc. 126. Solar Neutrinos and Neutrino Astronomy, Homstake, 1984,* ed. ML Cherry, K Lande, WA Fowler, p. 162. New York: Am. Inst. Phys. (1985)
72. Wolfendale AW, Young ECM, Davis R Jr. *Nature Phys. Sci.* 238:130 (1972)
73. Singer P. *Springer Tracts Mod. Phys.* 71:39 (1974)
74. Bilokon H, et al. *J. Geophys. Res.* 94:12, 145 (1989)
75. Charalambus S. *Nucl. Phys. A* 166:145 (1971)
76. Suzuki T, Measday DF, Roalsvig JP. *Phys. Rev. C* 35:2212 (1987)
77. Florkowski T, Morawska L, Rozanski K. *Nucl. Geophys.* 2:1 (1988)

78. Preusse W. *Höhenstrahlungsinduziertes Nulleffektspektrum von Gammastrahlungsdetektoren*. PhD thesis, TU Technical University Bergakademie, Freiberg (1993)
79. Heusser G. *Nucl. Instrum. Methods Phys. Res. B* 58:79 (1991)
80. Schröder WV, et al. *Z. Phys.* 268:57 (1974)
81. Heusser G. *Nucl. Instrum. Methods Phys. Res. B* 83:223 (1993)
82. Bunting RL, Kraushaar JJ. *Nucl. Instrum. Methods* 118:565 (1974)
83. Da Silva A, et al. *Nucl. Instrum. Methods Phys. Res.* A 354:553(1995)
84. Yamashita M, Stephens LD, Patterson HW. *Geophys. Res.* 71:3817 (1966)
85. Chen M, Novikov VM, Dougherty BL. *Nucl. Instrum. Methods Phys. Res. A* 336:232 (1993)
86. Cocconi G, Cocconi T. *Phys. Rev.* 84:29 (1951)
87. Belli PL, et al. *Nuovo Cimento* 101A:959 (1989)
88. Rindi A, et al. *Nucl. Instrum. Methods Phys. Res.* A272:87 (1988)
89. Aglietta M, et al. *Nuovo Cimento* 12C:467 (1989)
90. Heaton R, et al. *Nucl. Instr. Methods Phys. Res.* A267:529 (1989); *Nucl. Geophys.* 4:499 (1990)
91. Preusse W, Unterricker S. *Nucl. Instrum. Methods Phys. Res. B* 94:569 (1995)
92. Vojtyla P, Beer I, Stavina P. *Nucl. Instrum. Methods Phys. Res.* B86:380 (1994)
93. Vojtyla P. *Nucl. Instrum. Methods Phys. Res. B* 100:87(1995)
94. Crouch MF. *Proc. Int. Cosmic Ray Conf., 20th, Moscow*, 6:165 (1987)
95. Wordel R, Mouchel D. See Ref. 18, p. 141 (1994)
96. Shizuma K, et al. *Nucl. Instrum. Methods Phys. Res. B* 66:459 (1992)
97. Reeves JH, Arthur RJ. *J. Radioanal. Nucl. Chem.* 124:435 (1988)
98. McDaniel FD, et al. *Nucl. Instrum. Methods Phys. Res. B* 89:242 (1994)
99. Davis R Jr, Harmer DS, Hoffmann KC. *Phys. Rev. Lett.* 20:1205 (1968)
100. Wink R, et al. *Nucl. Instrum. Methods Phys. Res. A* 329:541 (1993)
101. Liu M, Lee HW, McDonald AB. *Nucl. Instrum. Methods Phys. Res. A* 329:291 (1993)
102. Pereira EB, Setzer AW, Cavalcanti IFA. *Radiat. Prot. Dosim.* 24:85 (1988) Howard AJ, Johnson BK, Strange WP, *Nucl. Instrum Methods Phys. Res. A* 293:589 (1990)
103. Wojcik M, Wlazlo W. *Nucl. Instrum. Methods Phys. Res. A* 345:351 (1994)
104. Schönhofer F. See Ref. 18, p. 155 (1994)
105. *Borexino at Gran Sasso, Proposal for a Real Time Detector for Low Energy Solar Neutrinos, Milano.* (1991)
106. Povinec P. *Proc. Int. Summer School, Low Measurements of Man-Made Radionuclides in the Environment, 2nd, Huelva, 1990*, ed. M Garcia-Leon, G Madurga. p. 38. Singapore:World Scientific (1991)
107. Watt DE, Ramsden D. *High Sensitivity Counting Techniques.* Intern. Series of Monographs on Electronics and Instrumentation, ed. DW Fry, W Higinbotham Oxford: Pergamon (1964)
108. Loosli HH, Oeschger H. *Proc. Int. Conf. Low Radioactivities, 2nd, High Tatras, 1980*, ed. P Povinec, p. 117. Bratislava: Veda (1982)
109. Moody JR, Lindstrom RM. *Anal. Chem.* 49:2264 (1977)
110. Brodzinski RL, et al. *Nucl. Instrum. Methods Phys. Res. A* 292:337 (1990)
111. Loosli HH, Heimann M, Oeschger H. *Radiocarbon* 22:461 (1980); Loosli HH, Forster M, Otlet RL. *Radiocarbon* 28:615 (1986)
112. Bodmann B, et al. *Nucl. Instrum. Methods Phys. Res. A* 286:214 (1990)
113. Arthur RJ, Reeves JH. J. *Radioanal. Nucl. Chem.* 160:297 (1992); Kamikubota N, et al. See Ref. 60, p. 275 (1992); Forster A, et al. *Phys. Lett. B* 138:301 (1984)
114. Reeves JH, et al. *IEEE Trans. Nucl. Sci.* 31:697 (1984)
115. Wogman NA, Perkins RW, Kaye JH. *Nucl. Instrum. Methods* 74:197 (1969); Alyoshin VI, et al. *Nucl. Instrum. Methods* 197:341 (1982); Kaye JH, et al. *Nucl. Instrum. Methods* 100:333 (1972)
116. Wogman NA, Robertson DE, Perkins RW. *Nucl. Instrum. Methods* 50:1 (1967); Heusser G. *Nucl. Instrum. Methods Phys. Res. B* 17:423 (1986)
117. Cooper JA, Perkins RW. *Nucl. Instrum. Methods* 99:125 (1972)
118. Kamikubota N, et al. *Nucl. Instrum. Methods Phys. Res. A* 245:379 (1986)
119. Morales A, et al. *J. Phys. G* 17:S211 (1991)
120. Goulding FS, et al. *IEEE Trans. Nucl. Sci.* 32:463 (1985); 31:285 (1984); Caldwell DO, et al. *Phys. Rev. Lett.* 54:281 (1985)
121. Caldwell DO. *J. Phys. G* 17:S137 (1991)
122. Avignone FT III, et al. *Phys. Rev. C* 34:666 (1986)
123. Davis R Jr. *Proc. Int. Symp. Neutrino Astrophysics, Frontiers of Neutrino Astrophysics, Takayama, 1992*, ed. Y Suzuki, K Nakamura, p. 47. Tokyo: Univ. Acad.

Press (1993)
124. Davis Jr R. *Proc. Informal Conf. on Status and Future of Solar Neutrino Research, BNL 50879*, p. 1. Upton, NY: Brookhaven Natl. Lab. (1978)
125. Fireman EL, et al. See Ref. 71, p. 22 (1985)
126. Kummer FH, Stoenner RW, Davis R Jr. *Construction of Miniature Low Level Proportional Counters, BNL 16972*. Upton, NY: Brookhaven Natl. Lab. (1972)
127. Pomanski AA. *Nucl. Instrum. Methods Phys. Res. B* 17:406 (1986)
128. Belotti E. *Nucl. Instrum. Methods Phys. Res. A* 264:1 (1988); Paoluzi L. *Nucl. Instrum. Methods Phys. Res. A* 279:133 (1989)
129. Henrich E, Ebert KH. *Angew. Chem. Int. Ed. Engl.* 31:1283 (1992)
130. Bahcall JN, Pinsonneault MH. *Rev. Mod. Phys.* 64:885 (1992)
131. Turck-Chièze S, Lopes I. *Astrophys. J.* 408:347 (1993)
132. Brookhaven National Laboratory. *Proposal to DOE for a Gallium Solar Neutrino Experiment, BNL-37081* (1985)
133. Anselmann P, et al. *Phys. Lett. B* 285:376 (1992)
134. Stolarczyk T. *Bruit de fond dans l'expérience GALLEX de détection de neutrinos solaires*, PhD thesis, Université de Paris-Sud (1990)
135. Ahlen SP, et al. *Phys. Lett. B* 249:149 (1990)
136. Wink R, et al. *Nucl. Instrum. Methods Phys. Res. A* 329:541 (1993)
137. Heusser G. *Trends in Astroparticle Physics*, ed. PCh Bosetti, p. 33. Leipzig: Teubner (1994)
138. Abdurashitov JN, et al. *Nucl. Phys. B* (Proc. Suppl.) 38:60 (1995)
139. Nakahata M. *Search for ^{8}B Solar Neutrinos at Kamiokande-II*, PhD thesis, Univ. Tokyo (1988)
140. Suzuki A. *KEK Preprint 88-65* (1988)
141. Suzuki Y. *Nucl. Phys. B* 35(Proc. Suppl.):273, 407 (1994)
142. Ewan GT. See Ref. 123, p. 147 (1993)
143. Jagam P, Wang JX, Simpson JJ. *J. Radioanal. Nucl. Chem.* 171:277 (1993)
144. Giammarchi MG. *Nucl. Phys. B* 35(Proc. Suppl.):433 (1994)
145. Ragavan RS, et al. *Design Concepts for Borex, Tech. Memo. 11131-880114-02TM*, AT&T Bell Lab. (1988); de Bari A, et al. *Radiopurity of the Borexino Scintillator, Tech. Memo. 11121-921015-37*, AT&T Bell Lab. (1992)
146. Kirsten T. *Proc. Int. Conf. Neutrino Physics and Astrophysics, 13th, Boston, 1988*, ed. J Schneps, et al, p. 742. Singapore: World Scientific (1989)
147. Moe MK. *Int. J. Mod. Phys.* E2:507 (1993); Moe MK. *Nucl. Phys. B* 19 (Proc. Suppl.):158 (1991); Avignone FT III, Brodzinski RL. *Prog. Part. Nucl. Phys.* 21:99 (1988)
148. Maier B. *Nucl. Phys. B* 35(Proc. Suppl.):358 (1994)
149. Petry F, et al. *Nucl. Instrum. Methods Phys. Res. A* 332:107 (1993)
150. Avignone FT, et al. *Nucl. Phys. B* 35(Proc. Suppl.):354 (1994)
151. Vuilleumier JC, et al. *Phys. Rev. D* 48:1009 (1993)
152. Elliot SR, Hahn AA, Moe MK. *Nucl. Instrum. Methods Phys. Res. A* 273:226 (1988)
153. Boehm F, et al. *Status Rep. on a New Anode and XY-Pad System of the Gotthard TPC Experiment, CALT-63-687* (1994)
154. NEMO Collaboration. *Nucl. Phys. B* 35(Proc. Suppl.):369 (1994); NEMO Collaboration. *Nucl. Instrum. Methods Phys. Res.* A 354:338 (1995)
155. Caldwell DO, et al. *Phys. Rev. Lett.* 61:510 (1988); Reusser D, et al. *Phys. Lett. B* 255:143 (1991); Morales J, et al. *Nucl. Instrum. Methods Phys. Res. A* 321:410 (1992); Beck M. *Nucl. Phys. B* 35(Proc. Suppl.):150 (1994)
156. BPRS (Beijing, Paris, Roma, Saclay) Collaboration. *Nucl. Phys. B* 35(Proc. Suppl.):159 (1994); Quency JJ, et al. *Phys. Lett. B.* 351:70 (1995)
157. Spooner NJC, et al. *Nucl. Phys. B* 35(Proc. Suppl.):162 (1994); Bacci C, et al. *Nucl. Phys. B* 35(Proc. Suppl.):165 (1994)
158. Sadoulet B. *Nucl. Phys. B* 35 (Proc. Suppl.):117 (1994)
159. Dougherty BL. *Proc. Snowmass 1994, Particle and Nuclear Astrophysics and Cosmology in the Next Millenium*, ed. R Peccei, E Kolb. Singapore: World Scientific. In press (1995)
160. Coron N, et al. *Nucl. Phys. B* 35(Proc. Suppl.):169 (1994)
161. Nucciotti A, et al. *Nucl. Phys. B* 35(Proc. Suppl.):172 (1994)
162. *Handbook of Semiconductor Wafer Cleaning Technology*, ed. W Kern. Park Ridge: Noyes (1993)